Langley Memorial Aeronautical Laboratory

LANGLEY SUB-LIBRARY

1115.5

UNCLASSIFIED

Copy 2

NATIONAL ADVISORY COMMITTEE FOR AERONAUTICS

NACA

CLASSIFICATION CANCELLED

ADVANCE CONFIDENTIAL REPORT

CLASSIFICATION CHANGED

To UNCLASSIFIED

By authority of NACA Status Book Date Dec. 1952

NB 8-16-54

EXPERIMENTAL INVESTIGATION OF A NEW TYPE OF LOW-DRAG WING-NACELLE COMBINATION

By H. Julian Allen and Charles W. Frick, Jr.

Ames Aeronautical Laboratory
Moffett Field, Calif.

CLASSIFIED DOCUMENT

This document contains classified information affecting the National Defense of the United States within the meaning of the Espionage Act, USC 50:31 and 32. Its transmission or the revelation of its contents in any manner to an unauthorized person is prohibited by law. Information so classified may be imparted only to persons in the military and naval Services of the United States, appropriate civilian officers and employees of the Federal Government who have a legitimate interest therein, and to United States citizens of known loyalty and discretion who of necessity must be informed thereof.

July 1942

To be returned to the files of the Langley Memorial Aeronautical Laboratory.

1115.5 N.A.C.A 35-215/1

~~CONFIDENTIAL~~ UNCLASSIFIED

E R R A T A

NATIONAL ADVISORY COMMITTEE FOR AERONAUTICS

ADVANCE CONFIDENTIAL REPORT

EXPERIMENTAL INVESTIGATION OF A NEW TYPE OF LOW-DRAG WING-NACELLE COMBINATION

By H. Julian Allen and Charles W. Frick, Jr.
Ames Aeronautical Laboratory
Moffett Field, Calif.

July 1942

Page 11, paragraph 3, line 10:

Change to read "is shown on figure 18 for three survey positions at 49 percent chord."

Figure 18:

Add "at 49 percent chord"

NATIONAL ADVISORY COMMITTEE FOR AERONAUTICS

ADVANCE ~~CONFIDENTIAL~~ REPORT

EXPERIMENTAL INVESTIGATION OF A NEW TYPE OF LOW-DRAG WING-NACELLE COMBINATION

By H. Julian Allen and Charles W. Frick, Jr.

SUMMARY

The results of an experimental investigation of two new-type low-drag wing-nacelle units suitable for use with pusher propellers are given. The test data support the fundamental design principles in indicating that

1. By making the nose of the nacelle and the leading edge of the wing coincident, the transition from laminar to turbulent flow at or near the common nose is avoided; and

2. By proper choice of the shape of the nacelle, the minimum pressure point and the pressure gradient are such that transition is made to occur at or behind the transition point on the wing.

The drag increments due to these nacelles are reduced to from one-half to two-thirds of that of conventional nacelle forms.

The introduction of the nacelle on the wing

1. reduced the critical speed as estimated from subcritical pressure measurements;

2. increased the maximum lift coefficient of the unit; and

3. produced no adverse effects on the lift and moment characteristics.

The measured subcritical pressure distributions indicate that the critical speed of the junction of such wing-nacelle units, using the "superposition method" of reference 1, will be conservatively predicted.

INTRODUCTION

In a boundary-layer investigation of a typical wing-fuselage combination (reference 2), it was found that at points distant from the junction of the wing and fuselage surfaces the transition point was well back of the wing leading edge. However, as the junction was approached, the transition point moved forward until at the surface junctions the transition point was at the leading edge of the wing. It is evident that this forward movement of the transition point promotes an increase in drag. This increase is due, in part, to the fact that a portion of the surface, which in the absence of the fuselage was subjected to only the small shear of a laminar boundary layer, is, in its presence, subjected to higher surface shears accompanying the turbulent boundary layer. Moreover, the increased shear over the forward surface of the airfoil promotes an increase in the boundary-layer thickness at the minimum pressure point. This in turn has an adverse effect on the recovery of pressure back of the minimum pressure point so that an additional pressure drag is experienced near the junction of the bodies.

The drag increase will clearly not be serious for the junction of a high fineness ratio body, such as the usual fuselage, with a wing having the conventional airfoil sections with their forward minimum pressure positions. However, for the combination of a low fineness ratio body, such as an ordinary nacelle, with a low-drag wing, the drag increase may assume considerable importance. This follows because the forward movement of the transition at the junction subjects a greater portion of the surface to the higher shear accompanying turbulent flow, and because the adverse gradient aft of minimum pressure point is of necessity greater and the pressure recovery on both wings and nacelle near the junction is less complete.

A method for preventing such premature transition and the resulting interference drag is presented in this report. Experimental results of an investigation of a combination of a wing and short body of revolution designed to prevent such interference are presented. In the course of the experiments, pressure distribution measurements were made on the wing alone, at the wing-nacelle junction and along the top and bottom meridian of the nacelle. These data for the wing-nacelle junction permitted a comparison of the observed pressures at the junction with those calcu-

lated by the "superposition method" of reference 1, an approximate method that is commonly employed in estimating the critical compressible speed at the junction of two bodies.

THEORY

Consider the midwing combination of an airfoil with a body of revolution wherein the nose of the body of revolution protrudes forward of the leading edge of the airfoil. Progressing from the nose of the body along the surface toward the leading edge of the wing, it is evident that although the pressure falls aft of the body nose, it must rise as the stagnation point on the leading edge of the wing is approached. In consequence, the laminar boundary layer which starts at the nose of the body thickens unduly and becomes separated as it approaches the wing stagnation point. In the usually important Reynolds number range this unstable separated laminar layer then degenerates into a turbulent boundary layer. A similar transition to turbulence occurs near the nose of the body for a combination wherein the leading edge of the wing is forward of the nose of the body of revolution.

If, in such a combination, the nose of the nacelle and the leading edge of the wing are coincident, then no unfavorable gradient exists near the nose of either and hence transition to turbulent flow at the common nose should not occur. Moreover, if the airfoil and body of revolution are properly matched so that in combination the minimum pressures occur at the same chordwise station, and the favorable gradients ahead of the minimum pressure points are such as to maintain the same boundary layer Reynolds number along the spanwise line of minimum pressures, the resulting combination should maintain low drag throughout the low-drag Reynolds number range for the wing alone.

DESCRIPTION OF MODEL

To investigate the validity of this method for preserving laminar flow at the junction and obtaining a low-drag combination, the test of a specific wing-nacelle combination was undertaken. The model selected was a simple midwing combination of a typical low-drag airfoil with a short body of revolution.

The NACA 35-215 airfoil, selected for the wing section, was chosen because high Reynolds number free-flight data for this profile are available (reference 3). It was considered that these data would allow prediction of the probable performance of the wing-nacelle unit in free flight from a knowledge of test results, especially of the low-drag Reynolds number range of the combination.

The estimated wind-tunnel turbulence and the maximum tunnel speed indicated that a wing of 4-foot chord, the ordinates of which are given in table I, would give an effective Reynolds number range equivalent to the low-drag range in some full-scale applications of this profile. The wind-tunnel turbulence was found to be somewhat lower than expected and the surface conditions of the wing were such that the maximum Reynolds numbers attainable were still in the low-drag range.

An analysis of the flight data of reference 3 indicated that with similar surface conditions, the low-drag characteristics of this wing could be maintained at a Reynolds number of 20 million (2×10^7). Consideration of a typical flight application, assuming speed (400 mph) and altitude (20,000 ft) consistent with modern design, permitted a wing chord of 8 or 9 feet. Assuming an air-cooled engine 4 feet in diameter, the ratio of nacelle diameter to wing chord is one-half. The length was made one and one-half times the wing chord for a propeller location 30-percent wing chord behind the wing trailing edge. Hence the fineness ratio of the nacelle selected was 3-1/3.

Matching of the nacelle of 3-1/3-fineness ratio with the 35-215 wing was performed in such a manner as to give

1. a minimum pressure position 33-1/3 percent of the length from the nose (coincident with the minimum pressure position on the wing when combined), and

2. a pressure gradient ahead of minimum pressure such as to give a gradient for the combination sufficiently favorable to promote approximately the same length of laminar run as on the surface of the wing alone. It should be clear that, for the combination, the length of the laminar run is prone to be least in the immediate neighborhood of the junction of the wing and nacelle surfaces. This follows because the "crowding" effect of the proximity of the surfaces of the streamlines acts to increase the boundary-layer thickness and tends to promote earlier transition to

turbulent flow. Accordingly, to determine the suitability of a particular nacelle in combination with the wing, the length of the laminar run at the junction of the surfaces only need be determined.

It was realized that the desired body of revolution, which when combined with the wing would meet these requirements, was one on which the maximum velocity should also be reached at a point one-third of the body length aft of the nose as measured along the axis. Moreover, the slope of the velocity-distribution curve ahead of the maximum velocity point should have the following characteristics:

1. A positive slope for all points ahead of the maximum velocity point.

2. A nearly constant slope from a point somewhat aft of the nose to the maximum velocity position.

3. The slope over this section of the body should be sufficiently favorable to permit the value of R_δ for the body of revolution at the maximum velocity position to be not more than that for the wing at its maximum velocity position. This required the value of R_δ^2/R_L for the body of revolution at the maximum velocity position, as calculated by the method of reference 4, to be less than c/L (that is, two-thirds) of the value of R_δ^2/R_c for the wing at its maximum velocity position. In the above, c is the wing chord, L is the length of the body of revolution, R_c is the wing Reynolds number based on the wing chord and stream velocity, R_L is the body Reynolds number based on the body length and stream velocity, and R_δ is the boundary-layer Reynolds number for the wing or body boundary layer as the case may be, based on the boundary-layer thickness and the local velocity outside the boundary layer at the maximum velocity position.

Experience indicated that such a nacelle shape would be one generated by a source-sink system having a nearly uniform distribution of sources up to the axial position corresponding to the maximum velocity point followed by any not-too-abruptly changing distribution of sinks. Accordingly, a source-sink system having a uniform source distribution up to the maximum velocity point followed by a uniform sink distribution was considered, and the shape and velocity distribution were calculated by the method of reference 5. This velocity distribution satisfied sufficiently the shape requirements.

Using the superposition method of reference 1 for combining velocities, the velocity distribution along the wing-nacelle junction was calculated and the value of R_δ^2/R_c was determined for the junction at the maximum velocity position on the assumption that the two-dimensional equation for R_δ^2/R_c, as given in reference 4, applied. This value was considerably less than for the wing alone, so that it was believed that the adverse "crowding" effect on the boundary layer at the junction due to the proximity of the wing and nacelle, not considered in the calculation, would be very nearly compensated for.

Because this nacelle, when combined with this typical low-drag section, appeared to be a satisfactory combination, it was decided to classify this type of nacelle as of "Series 1," this particular nacelle being the NACA 133-30. In this system of nomenclature, the first number of the first group represents the series, the second two numbers give the minimum pressure position along the axis in percent of the length, and the two numbers in the second group following the hyphen give the maximum diameter in percent of the length.

Unfortunately, changing the general intensity of the sources and sinks in a given source-sink system will promote shapes differing not only in their thickness ratios but also in their thickness distribution. However, for moderate changes of the source-sink intensity, the change in the thickness distribution is small, so that this device may be used to obtain a first approximation to the shape and velocity distribution for nacelles of other thickness ratios. The shape and velocity distribution for the NACA 133-18 nacelle was calculated as a first approximation by changing the general source-sink intensity. Consideration of the difference between this "near" shape and the "true" shape determined a revised source-sink distribution which permitted, as a close second approximation, the velocity distribution to be determined. Using the calculated results for the 18-percent- and 30-percent-thick nacelles, the velocity distributions over the 14-, 22-, 26-, and 34-percent-thick nacelles of this series were obtained by interpolation or extrapolation. These results are given in table II.

One of the nacelles investigated in these tests is the afore-mentioned NACA 133-30. The ordinates of the model are given in table III, and the wing-nacelle unit is

shown in figures 1 to 3, inclusive. The ideal lift coefficient of the NACA 35-215 profile occurs at a wing angle of 1.00° so that the wing was set at 1.00° incidence with respect to the axis of the nacelle.

It was believed that the blunt tail of the Series 1 nacelle might incur an unnecessary increase in form drag. Accordingly, it was decided to test a pointed-tail-model nacelle having a similar velocity distribution to that for the Series 1 nacelle. This was accomplished by building the blunt-tailed nacelle such that at a point along the axis of revolution 60 inches from the nose the tail cone could be removed and a pointed-tail cone, somewhat longer, substituted. The second nacelle was designated as a Series 2 nacelle. This particular model nacelle designation was by virtue of its increased length, NACA 230-28. The ordinates of this model are given in table IV, and photographs of the resulting wing-nacelle unit are shown in figures 4 and 5. The wing incidence again was 1.00° with respect to the axis of the nacelle.

By comparison with the Series 1 nacelles, the velocity distribution from the nose to a point somewhat aft of the maximum velocity point was determined for this series of nacelles and is given in table V along with the ordinates of the shape.

The pressure orifices located in the wing were placed along the surface so that when the nacelle was mounted on the wing the line of orifices was 1/2 inch away from the junction of the wing and the nacelle surfaces. The same orifices sufficed for the pressure measurements on the wing alone. Pressure orifices were also provided along the top and bottom meridian lines of the nacelle. In all cases the pressure orifices were 0.020-inch diameter flush with the surface.

Pressures over the nacelle 45° section and over the wing 10 inches outboard of the junction were measured with a single static tube "mouse."

DESCRIPTION OF APPARATUS

Tests of the NACA 35-215 wing, the NACA 35-215 wing-NACA 133-30 nacelle combination, and the NACA 35-215 wing-NACA 230-28 nacelle combination were made in the 7- by

10-foot tunnel of the Ames Aeronautical Laboratory. This tunnel is of the closed-throat, rectangular-section, single-return type, capable of airspeeds of 300 miles per hour. The turbulence level of the air stream and the surface conditions of the model were such that low drag was obtained at the maximum attainable Reynolds number.

The wing alone and the wing-nacelle combination were tested as "through" models. The 6-foot span of the wing was mounted across the 7-foot dimension of the test section, 6-inch span dummy ends being used to give two-dimensional flow. Clearance of 1/32 inch between dummy end and wing was maintained during all tests as this clearance was believed critical in its effect on minimum drag and maximum lift of the wing.

Spanwise drag surveys of the wing were made with a momentum rake prior to actual test and the surface was finished until aerodynamically smooth. Care was taken to preserve this surface for all free transition tests. A half-inch-wide strip of No. 60 carborundum grains was used to fix transition in all tests designated "with fixed transition."

Boundary-layer surveys and some pressure-distribution data were obtained by use of a "mouse" composed of five total-head tubes and a single static tube. Pressure tubes from the "mouse" were taken into the wing through a small hatch and conducted to a multiple-tube manometer through a channel in the wing.

TESTS AND TEST RESULTS

The surface of the wing was finished until spanwise wake surveys indicated that the section drag was constant over the center 4 feet of the span. Further refinishing did not reduce the drag at any section. A check of the ideal angle was made by wake surveys of the drag at the center of the span.

The results presented herein are based on a wing chord of 4 feet, a wing area of 24 square feet, and a projected frontal area of 2.58 square feet for the nacelle.

All test results excepting pressure distributions have been corrected for the interference of the tunnel walls.

The effect of fluid compressibility on the interference has not been considered because, even at the highest Mach numbers, the error is less than 0.0001 for the drag coefficients and approximately one-half of 1 percent for the lift, moment, and angle of attack. The effect of the known downstream pressure gradient on the wing was negligible. The corrected coefficients for the wing are obtained from the following, the primes indicating the test results:

$$c_d = 0.977\, c_d'$$

$$c_l = 0.949\, c_l'$$

$$c_{mc/4} = 0.982\, c_{mc'/4} + 0.0081\, c_l'$$

$$\alpha = \alpha' + 0.298\, [c_l' + 4\, c_{mc'/4}] \text{ (deg)}$$

$$R = 1.009\, R'$$

$$M = 1.009\, M'$$

The addition of the nacelle does not materially affect the corrections except that the tunnel pressure gradient is no longer negligible. The drag results of the wing-nacelle unit are corrected by

$$c_d = 0.977\, c_d' + 0.0004$$

The other corrections remain the same.

Section characteristics of the 35-215 profile throughout the wing-angle range at a tunnel Reynolds number of 5.75 million, are given on figure 6. The lift and quarter-chord-moment coefficients were computed from pressure distributions taken at the center of the span. The drag coefficients were computed from wake surveys at the same position after the pressure orifices were sealed.

The effects of the gap between the wing and dummy end on the drag of the wing are shown in figure 7. Drag coefficients, as measured by a force balance, are compared with drag coefficients calculated from wake surveys at the span center line. Both sets of data were obtained at a test Reynolds number of 5.75 million and are plotted against wing angle of attack and force-test lift coefficient.

The results of wake drag measurements at the center of

the span throughout a test Reynolds number range of 1.5 million to 10 million at 0°, 1°, 2°, and 4° angles of attack, are shown in figure 8. These tests were run simultaneously with force tests of the wing so that tares for determining the drag increment due to the nacelle were obtained.

The force-test drag coefficients are given in figures 9 to 12, inclusive, for approximately 0°, 1°, 2°, and 4° angles of attack, respectively. These figures also show force-test drag coefficients for the wing combined with the NACA 133-30 nacelle and with the NACA 230-28 nacelle as functions of the test Reynolds number. In addition, figures 9 and 10 show force-test drag coefficients for 0° and 1° for the wing, combined with the NACA 133-30 nacelle with transition fixed with carborundum strips in the wing-nacelle surface junctions. These tests were run to simulate the drag experienced by such a wing-nacelle combination when premature transition occurs in the surface junctions. The transition fixing strips extended from the nose in a 15° V shape along the junction to about 15-percent chord. From 15-percent to 40-percent chord, the strips were of constant width. These results are designated "transition fixed in junction."

The drag-coefficient increment due to the nacelles, derived from the results presented in figures 9 to 11, inclusive, but based on the nacelle projected frontal area, are given in figure 13 for 0°, 1°, and 2° as functions of the test Reynolds number. Increment drag coefficients with "transition fixed in nose junction" are also given for 0° and 1°.

Figure 14 presents the section drag coefficient for the wing alone and for the wing and NACA 133-30 nacelle combined, as obtained by adding the drag increment due to the nacelle, based on the wing area, to the wing section drag. Drag coefficients for both are given as a function of angle of attack, as well as section lift coefficient for test Reynolds numbers of 4, 6, and 10 million.

The results of spanwise wake surveys are shown on figure 15. Those for the wing-nacelle (NACA 133-30) were made at test Reynolds numbers of 5 and 10 million. All spanwise surveys of the wing were made at a test Reynolds number of 8.5 million.

Results of force tests of the lift, drag, and moment

throughout the angle-of-attack range at a test Reynolds number of 3.25 million are presented in figure 16, both for the wing alone and the wing-nacelle (NACA 133-30). Similar tests for the combination with the NACA 230-28 nacelle were made but with negligible difference in results. Tests at Reynolds numbers of 5 and 6 million also showed minor differences.

In order to arrive at some idea of the spanwise variation of lift due to the presence of the nacelle, lift coefficients, integrated from pressure distributions taken at the nacelle center line and nacelle wing juncture, are plotted across the span on figure 17. Portions of the curves were adjusted to give an average lift coefficient for the span equivalent to that obtained in the force tests previously mentioned (fig. 16).

Extensive boundary-layer surveys with a small "mouse" were made at positions from 80-percent to 40-percent wing chord on the wing alone for test Reynolds numbers of 1.5 to 10 million. Similar surveys were made for the wing-nacelle (NACA 133-30) unit 10 inches outboard of the junction, in the wing-nacelle junction, on the nacelle 45° line, and on the nacelle top meridian. The variation of δ, the boundary-layer thickness, with test Reynolds number at the wing ideal angle taken from the measured profiles, is shown on figure 18 for the three survey positions. The theoretical variation of δ with Reynolds number, calculated from experimental pressure distributions by the method of Jacobs and Von Doenhoff (reference 4), is also given for these positions.

Other boundary-layer studies relating to the location of the point of transition from laminar to turbulent flow were made with a mouse composed of a single-surface total-head tube and a single static tube. The results of these tests for the wing-nacelle (NACA 133-30) are shown on figures 19 and 20 for 0° and 1° wing angles of attack. The location of transition across the span is indicated for test Reynolds numbers of 2, 5, 8, and 10 million.

Pressure distributions over the wing throughout the angle-of-attack range were obtained at a test Reynolds number of 5.75 million and Mach number of 0.20. These data are presented in uncorrected form in table VI. Other pressure distributions over the wing were taken for 0°, 1°, 2°, and 4° angles of attack throughout a Reynolds number range of 1.5 to 10 million but showed little variation

with Reynolds number and consequently are not given. The pressure distribution for the wing at the ideal lift corrected for Mach number is given on figure 21.

Similar tests were made for the wing and NACA 133-30 nacelle combination. The pressures along the wing-nacelle junction are given in table VII for stations in percent wing chord. These data are for a test Reynolds number of 5.75 million and for a Mach number of 0.20. Pressures over the nacelle top and bottom meridian are given in table VIII for stations in percent nacelle length for the same Reynolds number and Mach number.

Figure 22 presents the experimental velocity distribution over the 35-215 profile, as obtained from the pressure distribution shown on figure 21. The theoretical velocity distribution for the NACA 133-30 nacelle is also given in terms of wing chord. The superposition method is applied to predict the velocity distribution for the wing-nacelle junction for both upper and lower surfaces. The superposed velocity distributions are shown by the dashed lines.

Experimental velocity distribution obtained from pressure measurements in the wing-nacelle (NACA 133-30) junction are compared on figure 23 with the velocity distribution predicted by superposition. The experimental data are given for Reynolds numbers of 5 million and 8.3 million, both corrected to zero Mach number so that only Reynolds number variation is shown.

To extend the better agreement found at higher Reynolds numbers to the critical Reynolds number, pressure-distribution tests of the wing-nacelle (NACA 133-30) junction, with transition fixed spanwise at 0.5-chord position, were made. Results of these tests, which showed no variation with Reynolds number, are given also on figure 23.

DISCUSSION

A discussion of the results of the drag tests in figures 9 to 12, inclusive, necessarily must consider to what extent placing a large nacelle on the wing will influence the flow characteristics caused by the gap between the wing and the dummy ends. Under certain conditions when the effect of the gap on the wing drag is large, especially where the wing experiences a change in the flow regime

as at 4° angle of attack, any variation in flow caused by the nacelle may result in large changes in the apparent nacelle drag increment. In fact, at this angle at the highest Reynolds numbers, as seen in figure 12, the negative drag-coefficient increment, as determined by force tests, was so large that when added to the wake-measured drag coefficient of the wing alone, the apparent drag coefficient, as seen in figure 14, was considerably less than that for the wing alone. At 0°, 1°, and 2° angle the effect is considered to be negligible, except perhaps at the higher Reynolds numbers where the increment due to the addition of the nacelle appears abruptly to become too small.

The increment drag-coefficient increase, in terms of the projected frontal area of the nacelle, at the ideal angle of attack (approximately 1°) is seen in figure 13 to vary from 0.021 at the lower test Reynolds numbers to probably 0.018 at the higher test Reynolds numbers. At the neighboring angles of attack of 0° and 1°, the increment drag coefficients for both nacelles are seen to remain low; however, the NACA 230-28 nacelle at these angles appears to be slightly superior to the NACA 133-30 nacelle. These low-drag coefficients are entirely in keeping with the results of transition location measurements shown in figures 19 and 20, which demonstrate that premature transition to turbulent flow was prevented.

Transition measurements on the wing alone and on the wing-nacelle (NACA 133-30) unit in the junction indicated that both would attain their lowest drag coefficients at the same Reynolds number. From the flight test results of the NACA 35-215 airfoil given in reference 3, it is considered that the lowest drag coefficient for this section with the same surface conditions will occur at a Reynolds number of approximately 22 million. Hence it is concluded that both wing-nacelle units with the same surface conditions would also attain their lowest drag coefficients at about this Reynolds number and that the corresponding increment drag coefficient would be approximately 0.016 in terms of the projected frontal area of nacelle.

Past experience has indicated that a fair value of the drag coefficient of an airfoil at Reynolds numbers of the order of 10 million may be found by considering the area ahead of the minimum pressure point to have a drag coefficient per square foot of surface of 0.0005 when subjected to laminar flow, and aft of minimum pressure 0.0034 when subjected to turbulent flow, or to a separated laminar flow

followed by turbulent flow. As an example such a method would predict a drag coefficient of 0.0039 for the wing alone, which is in excellent agreement with the results of these tests. The same method would predict an increment drag coefficient due to the nacelle of 0.014, based on the projected frontal area of the nacelle, which is in reasonably satisfactory agreement with the test results.

To determine the effect of premature transition on the drag, an attempt was made to "fix" transition at the 2-percent chord position aft of the leading edge in the four junctions of wing and nacelle (NACA 133-30) surfaces with small spheres (approximately 3/16-inch diameter) affixed to the surface. The effect on the drag coefficient in terms of the plan form area was about 0.0004 and it was concluded that, because of the markedly favorable pressure gradient in this vicinity, perhaps these balls had not reversed the local pressure gradient sufficiently to promote transition to turbulent flow. Accordingly, the balls were replaced with strips of carborundum-coated cellophane tape spread in a 15° V (approximately the "mixing length" angle) in the four corners and running about 15-percent-chord in the direction of the air flow. This increased the drag coefficient about 0.0010. An attempt was made to determine whether or not transition had been fixed at the nose by these strips but, because of the thin boundary layer in the favorable pressure gradient, the boundary-layer profile could not be measured accurately enough to allow any conclusions to be reached. Finally the carborundum strip was extended to 40-percent chord. The effect on the drag is shown on figures 9, 10, and 13 on the curves marked "wing + NACA 133-30 nacelle with transition fixed in junction." Experience has shown carborundum to be an effective means for fixing transition but this experience has been obtained from experiments on two-dimensional bodies having only moderately favorable pressure gradients. In consequence it cannot be stated definitely whether or not transition was fixed at or very near the beginning of the junction with the carborundum V strips. The failure of the spheres and the carborundum strips to increase the drag appreciably may be due to the peculiar three-dimensional flow in the junction, which is not well understood.

Boundary-layer "cross flow," a phenomenon of considerable interest which was observed in these tests, arises in the following manner. The pressures near the wing-nacelle junction are lower than at corresponding spanwise points on the wing sections distant from the nacelle. In conse-

quence the low-velocity boundary-layer air near the surface is caused to flow toward this region of lower pressure. This cross flow will be more pronounced the thicker the boundary layer and will be most marked for separated boundary layers which, per se, are subject to negligible shears in the flow direction. The wake surveys of figure 15 show the existence of the cross flow, which is seen to be most severe at the lower Reynolds numbers where the separated boundary-layer region aft of minimum pressure is most extensive.

It should be noted that when inter-boundary-layer cross flow exists, the wake method does not permit section drag characteristics to be obtained, since the wake under such conditions may include boundary-layer air from neighboring sections on the one hand or, on the other hand, may not include all the boundary-layer air from the section under consideration. That this occurred in the present investigation is shown in figure 15, wherein the apparent section drag coefficients of the sections immediately adjacent to the nacelle are absurdly low.

It is considered that inter-boundary-layer cross flow is also responsible for the fact that the maximum lift coefficient attained by the wing-nacelle unit is higher than for the wing alone as shown by figure 16. The pressure-distribution measurements showed that the lift on the nacelle and at the wing-nacelle junction did not account for the increase as seen in figure 17. It follows that the outboard airfoil sections attained higher maximum lift coefficients in the presence of the nacelle which would indicate that the cross flow in effectively providing boundary-layer control by draining off the low-energy boundary layer on the upper surface of the outboard sections improved the maximum lift of these sections.

Boundary-layer surveys indicated that on the wing alone and on the top meridian of the nacelle the laminar profiles were of the Blasius type. At the wing junction the profiles were not of the usual shape in that some slight influence of fluid friction extended far out from the surface. This was to be expected, since in progressing away from the surface of the wing (or nacelle), while the influence of the wing (or nacelle) surface abates, the influence of neighboring nacelle (or wing) surface remains. It was not considered that any of the measured profiles would be of sufficient interest to warrant their inclusion in the report.

As seen in figure 18, the measured boundary-layer thicknesses on the wing alone and on the top meridian of the nacelle agree well with those calculated by the method of reference 4. The boundary layer in the junction is, as would be expected, considerably thicker than on the wing alone. Moreover, this boundary layer appears to be considerably more stable than the usual wing laminar boundary layers which may be a result of the "guiding" influence of the V surface. Unfortunately the model Reynolds number could not be made high enough to study the aerodynamic characteristics with natural transition ahead of the minimum pressure point.

The curves of figures 6 and 16 indicate that for this airfoil section, with the wing alone and perhaps the wing-nacelle unit, a slight shift in the moment coefficient accompanies the transition from the low-drag to the higher-drag attitude, but this shift is in the opposite and favorable direction to that usually experienced on low-drag airfoils with minimum pressure farther back along the chord. This small moment shift was practically the same at all test Reynolds numbers. No accompanying shift in the curve of lift against angle of attack was apparent, as seen in these figures.

Within the small range of test Mach numbers available the calculated effect of fluid compressibility on the pressure distribution over the wing alone, as given by the von Kármán-Tsien equation (reference 6), as well as the less exact Glauert-Prandtl relation (reference 7), was found to satisfactorily explain the observed differences in the distributions within the experimental accuracy.

By the "method of small perturbations" (reference 6), it has been shown that the Glauert-Prandtl relation should apply as well to three-dimensional bodies. The experimental pressure distributions along the wing-nacelle junction shown in figure 23, which have been so corrected, do not precisely coincide. It is considered that this discrepancy is again a result of inter-boundary-layer cross flow. The lower surface pressures occur at the lower Reynolds numbers since then the cross flow is greater, so that the effective thickness ratio is less. That this would appear to explain the discrepancy is shown by the fact that by fixing the transition at close to the 0.5-chord position, the measured pressures were further diminished.

On figure 23 the junction pressure distribution calculated by the "superposition method" of reference 1, based on the theoretical nacelle and experimental wing pressure distributions, is shown. This calculated distribution, based on relatively crude assumptions, is seen to be in reasonably good agreement with the measured pressures. The discrepancies that exist are seen to be largely the result of the inter-boundary-layer cross flow. These results indicate that the use of the superposition method in predicting the critical Mach number will yield a conservative estimate, and that the estimate will be satisfactory if transition to turbulent flow occurs at or slightly aft of the minimum pressure position. In the present instance the predicted critical Mach number based on the calculated minimum pressure is 0.57, based on the experimental minimum pressure with transition fixed at 0.5 chord is 0.58, and based on the experimental minimum pressure with transition free at 8.3 million Reynolds number is 0.59. The tendency to low critical Mach numbers is unfortunately a characteristic of these low-drag wing-nacelle units as the minimum pressure positions of the wing and nacelle are purposely made coincident. The situation is aggravated in the present instance by the low-fineness ratio of the nacelle but it is anticipated that such low-fineness-ratio nacelles will in general be employed only for pusher-propeller engine units, in which case air induction at the nose will serve to reduce the maximum negative pressure and so increase the critical Mach number. A model wing engine nacelle unit suitable for pusher-propeller installation is under construction for test in the 7- by 10-foot tunnel. This model, equipped for nose air induction, is similarly designed to prevent premature transition to turbulent flow in the wing-nacelle junctions. It is planned to measure the junction pressure distributions so as to obtain quantitative results on the effect of internal air flow on the critical Mach number.

CONCLUSIONS

The results of the tests of these wing-nacelle units show that

1. By making the nose of the nacelles and the leading edge of the wing coincident, the transition from laminar to turbulent flow at or near the common nose may be avoided; and

2. By so shaping the nacelle that the chordwise location of the minimum pressure point on the nacelle is coincident with that for the wing, and by making the pressure gradient ahead of the minimum pressure point sufficiently favorable,

transition may be maintained at or back of the spanwise line of minimum pressures up to as high Reynolds numbers as for the isolated wing. In consequence, the drag increment due to the nacelles is reduced to from one-half to two-thirds of that for the usual nacelle form wherein these conditions are not fulfilled.

The introduction of the nacelles on the wing

1. reduced the critical speed as estimated from subcritical pressure measurements,

2. made possible an increase in the maximum lift coefficient of the unit, and

3. produced no adverse effects on the lift and quarter-chord moment characteristics.

The measured subcritical pressure distributions indicate that the critical speed of the junction of such wing-nacelle units, using the superposition method of reference 1, will be conservatively predicted.

Other experimental investigations (reference 2) of nose openings for air induction in low-drag bodies have shown that provided such openings are properly formed, the low-drag properties of the body may be maintained. Hence it is concluded that this method for maintaining low drags at the junction of two aerodynamic bodies may be applied generally to wing-nacelle units with nose openings (pusher propeller engine units, military armament) as well as without nose openings (landing gears).

Because of the high turbulence level in a propeller slipstream it is not considered that this method for maintaining low drags may be applied to wing-nacelle combinations housing tractor propeller engine units.

The drag of the wing-nacelle unit was, in the present instance, largely accounted for by the frictional drag of the laminar- and turbulent-flow areas. It would accordingly appear advisable when housing a propulsion unit or a

landing-gear unit, for example, to provide separate nacelles for each (compressibility effects permitting), rather than to lengthen one nacelle to provide housing for both units. The former method, providing the least turbulent area even though the total area is greater, should produce the least drag.

Ames Aeronautical Laboratory,
National Advisory Committee for Aeronautics,
Moffett Field, Calif.

REFERENCES

1. Robinson, Russell G., and Wright, Ray H.: Estimation of Critical Speeds of Airfoils and Streamline Bodies. NACA A.C.R., March 1940.

2. Becker, John V.: Wind-Tunnel Tests of Air Inlet and Outlet Openings on a Streamline Body. NACA A.C.R., Nov. 1940.

3. Wetmore, J. W., Zalovcik, J. A., and Platt, Robert C.: A Flight Investigation of the Boundary-Layer Characteristics and Profile Drag of the NACA 35-215 Laminar-Flow Airfoil at High Reynolds Numbers. Confidential Memorandum Report for Army Air Corps, May 1941.

4. Jacobs, E. N., and von Doenhoff, A. E.: Formulas for Use in Boundary-Layer Calculations on Low-Drag Wings. NACA A.C.R., Aug. 1941.

5. Prandtl, L.: Applications of Modern Hydrodynamics to Aeronautics. Rep. No. 116, NACA, 1921.

6. von Kármán, Th.: Compressibility Effects in Aerodynamics. Jour. of the Aero. Sci., July 1941.

7. Glauert, H.: The Effect of Compressibility on the Lift of an Aerofoil. R. & M. No. 1135, British A.R.C., 1927.

TABLE I

Ordinates of NACA 35-215 Wing. a = .50

Upper Surface				Lower Surface			
X Distance Along Chord		Y Ordinate		X Distance Along Chord		Ordinate	
Percent C	Inches	Percent C	Inches	Percent C	Inches	Percent C	Inches
0	0	0	0	0	0	0	0
0.376	0.18	1.137	0.55	0.624	0.30	-0.999	0.48
0.609	0.29	1.403	0.67	0.891	0.43	-1.209	-0.58
1.087	0.52	1.828	0.88	1.413	0.68	-1.534	-0.74
2.308	1.11	2.544	1.26	2.692	1.29	-2.026	-1.01
4.784	2.30	3.711	1.78	5.214	2.50	-2.829	-1.36
7.276	3.49	4.534	2.18	7.722	3.71	-3.346	-1.61
9.777	4.69	5.215	2.50	10.223	4.91	-3.763	-1.81
14.788	7.10	6.328	3.04	15.212	7.30	-4.432	-2.13
19.809	9.51	7.200	3.46	20.191	9.69	-4.952	2.38
24.838	11.92	7.889	3.79	25.162	12.08	-5.361	-2.57
29.873	14.34	8.408	4.04	30.127	14.46	-5.672	-2.72
34.913	16.76	8.770	4.21	35.087	16.84	-5.884	-2.82
39.958	19.18	8.967	4.30	40.042	19.22	-5.995	-2.88
45.009	21.60	8.977	4.31	44.991	21.60	-5.981	-2.87
50.077	24.04	8.732	4.19	49.923	23.96	-5.792	-2.78
55.130	26.46	8.109	3.89	54.869	26.34	-5.323	-2.56
60.150	28.87	7.262	3.49	59.850	28.73	-4.700	-2.26
65.150	31.27	6.283	3.02	64.850	31.13	-3.993	-1.92
70.137	33.67	5.228	2.51	69.863	33.54	-3.246	-1.56
75.113	36.05	4.140	1.99	74.888	35.95	-2.488	-1.19
80.086	38.44	3.062	1.47	79.914	38.36	-1.756	-0.84
85.056	40.83	2.042	0.98	84.944	40.77	-1.084	-0.52
90.029	43.21	1.134	0.54	89.971	43.19	-0.520	-0.25
95.009	45.60	0.424	0.20	94.991	45.60	-0.136	-0.07
100.000	48.00	0	0	100.00	48.00	0	0

TABLE II

Theoretical Velocity, $\frac{V}{V_o}$, Distributions over NACA Series 133 Nacelles for Various Maximum Diameter-Length Ratios

$\frac{X}{C}$	$\frac{r}{r_{max}}$	$\frac{D_{max}}{L}$=0.14	$\frac{D_{max}}{L}$=0.18	$\frac{D_{max}}{L}$=0.22	$\frac{D_{max}}{L}$=0.26	$\frac{D_{max}}{L}$=0.30	$\frac{D_{max}}{L}$=0.34
0	0	0	0	0	0	0	0
0.1250	0.2197	----	----	----	----	----	----
0.050	0.4369	0.985	0.971	0.955	0.936	0.916	0.895
0.075	0.5326	----	----	----	----	----	----
0.1000	0.6117	1.015	1.015	1.014	1.013	1.011	1.009
0.1500	0.7393	1.024	1.032	1.042	1.051	1.061	1.071
0.2000	0.8381	1.032	1.048	1.064	1.081	1.099	1.118
0.2500	0.9131	1.048	1.067	1.087	1.109	1.131	1.154
0.3000	0.9651	1.065	1.086	1.107	1.130	1.153	1.178
0.3500	0.9935	1.068	1.090	1.112	1.135	1.158	1.182
0.4000	0.9998	1.051	1.073	1.096	1.121	1.147	1.177
0.4500	0.9880	1.037	1.057	1.078	1.101	1.126	1.151
0.5000	0.9623	1.028	1.044	1.063	1.082	1.103	1.125
0.5500	0.9265	1.023	1.037	1.051	1.067	1.083	1.101
0.6000	0.8827	1.020	1.030	1.042	1.054	1.067	1.080
0.6500	0.8319	1.016	1.024	1.033	1.043	1.052	1.063
0.7000	0.7746	1.013	1.019	1.025	1.032	1.040	1.048
0.7500	0.7102	1.009	1.014	1.018	1.023	1.029	1.034
0.8000	0.6374	1.006	1.009	1.011	1.014	1.017	1.019
0.8500	0.5536	1.002	1.002	1.003	1.003	1.002	1.002
0.9000	0.4530	0.996	0.993	0.989	0.985	0.981	0.976
0.9500	0.3209	0.982	0.971	0.959	0.944	0.930	0.914
1.0000	0	0	0	0	0	0	0

TABLE III

Ordinates of NACA 133-30 Nacelle

x Distance along center line		r Radius	
Percent L	Inches	Percent L	Inches
0	0	0	0
1.250	0.90	3.318	2.39
2.500	1.80	4.680	3.37
5.000	3.60	6.598	4.75
7.500	5.40	8.043	5.79
10.000	7.20	9.238	6.65
15.000	10.80	11.164	8.04
20.000	14.40	12.656	9.11
25.000	18.00	13.789	9.93
30.000	21.60	14.573	10.49
35.000	25.20	15.002	10.80
40.000	28.80	15.098	10.87
45.000	32.40	14.919	10.74
50.000	36.00	14.532	10.46
55.000	39.60	13.991	10.07
60.000	43.20	13.329	9.60
65.000	46.80	12.563	9.05
70.000	50.40	11.697	8.42
75.000	54.00	10.725	7.72
80.000	57.60	9.626	6.93
85.000	61.20	8.360	6.02
90.000	64.80	6.841	4.93
95.000	68.40	4.846	3.49
100.000	72.00	0	0

TABLE IV

Ordinates of NACA 230-28 Nacelle

x Distance along Center Line		r Radius	
Percent L	Inches	Percent L	Inches
0	0	0	0
1.154	0.90	3.063	2.39
2.308	1.80	4.320	3.37
4.615	3.60	6.090	4.75
6.923	5.40	7.424	5.79
9.231	7.20	8.527	6.65
13.846	10.80	10.305	8.04
18.462	14.40	11.683	9.11
23.077	18.00	12.728	9.93
27.692	21.60	13.452	10.49
32.308	25.20	13.848	10.80
36.923	28.80	13.937	10.87
41.539	32.40	13.771	10.74
46.154	36.00	13.414	10.46
50.769	39.60	12.915	10.07
55.385	43.20	12.304	9.60
60.000	46.80	11.597	9.05
64.616	50.40	10.797	8.42
69.231	54.00	9.900	7.72
73.846	57.60	8.886	6.93
78.462	61.20	7.717	6.02
83.077	64.80	6.315	4.93
87.693	68.40	4.718	3.68
92.308	72.00	2.962	2.31
94.872	74.00	1.987	1.55
100.00	78.00	0	0

TABLE V

Theoretical Velocity, $\frac{V}{V_o}$, Distributions over NACA Series 230 Nacelles for Various Maximum Diameter-Length Ratios

$\frac{X}{C}$	$\frac{r}{r_{max}}$	$\frac{D_{max}}{L}=0.14$	$\frac{D_{max}}{L}=0.18$	$\frac{D_{max}}{L}=0.22$	$\frac{D_{max}}{L}=0.26$	$\frac{D_{max}}{L}=0.30$	$\frac{D_{max}}{L}=0.34$
0	0	0	0	0	0	0	0
0.0125	0.2282	----	----	----	----	----	----
0.0500	0.4542	0.987	0.973	0.956	0.935	0.912	0.890
0.0750	0.5526	----	----	----	----	----	----
0.100	0.6332	1.017	1.020	1.021	1.023	1.024	1.025
0.1500	0.7650	1.029	1.041	1.053	1.066	1.079	1.094
0.2000	0.8646	1.041	1.061	1.080	1.102	1.124	1.148
0.2500	0.9348	1.061	1.083	1.107	1.132	1.158	1.186
0.3000	0.9803	1.077	1.100	1.124	1.149	1.173	1.199
0.3500	0.9996	1.066	1.089	1.115	1.143	1.169	1.194
0.4000	0.9918	1.047	1.071	1.096	1.123	1.150	1.179
0.4500	0.9670	1.035	1.055	1.077	1.100	1.123	1.148
0.5000	0.9319	1.028	1.044	1.060	1.079	1.098	1.118
0.5500	0.8854	1.023	1.035	1.048	1.062	1.077	1.091
0.6000	0.8307	1.018	1.028	1.038	1.048	1.059	1.071
0.6500	0.7683	----	----	----	----	----	----
0.7000	0.6970	----	----	----	----	----	----
0.7500	0.6175	----	----	----	----	----	----
0.8000	0.5208	----	----	----	----	----	----
0.8500	0.4065	----	----	----	----	----	----
0.9000	0.2761	----	----	----	----	----	----
0.9500	0.1386	----	----	----	----	----	----
1.0000	0	----	----	----	----	----	----

TABLE VI - EXPERIMENTAL VALUES OF $\left(\frac{v}{V_o}\right)^2$ FOR NACA 35-215 WING*

Reynolds Number = 5.75×10^6 Mach Number = 0.20

C_{l_w} / α / %c	-0.448	-0.217	+0.012	0.138	0.243	0.357	0.478	0.688	0.879	1.060	1.220	1.305	1.386	1.418	1.428	0.670
	-5°	-3°	-1°	0°	1°	2°	3°	5°	7°	9°	11°	13°	15°	17°	19°	20°
								Upper Surface								
0	1.875	0.774	0.169	0	-0.014	0.047	0.206	0.838	1.713	3.013	4.287	5.659	6.621	7.128	7.528	1.720
0.38	0.052	0	0.189	0.383	0.639	1.009	1.397	2.427	3.483	4.846	6.130	7.313	8.222	8.553	8.735	1.909
0.60	0	0.063	0.333	0.558	0.823	1.196	1.582	2.578	3.515	4.753	5.881	6.948	7.720	8.161	8.393	1.776
1.08	0.021	0.219	0.549	0.761	1.028	1.372	1.715	2.587	3.359	4.391	5.426	6.399	6.130	6.415	6.568	1.726
2.31	0.218	0.481	0.825	1.007	1.242	1.527	1.798	2.460	3.008	3.624	4.328	4.846	5.146	5.268	5.243	1.719
4.79	0.477	0.732	1.020	1.171	1.344	1.558	1.836	2.215	2.562	3.055	3.438	3.750	3.912	3.956	3.887	1.698
7.27	0.626	0.859	1.126	1.259	1.406	1.571	1.745	2.096	2.382	2.733	3.041	3.240	3.384	3.392	3.310	1.662
9.77	0.738	0.951	1.199	1.309	1.434	1.574	1.725	2.021	2.283	2.563	2.811	2.960	3.071	3.053	2.950	1.692
14.79	0.888	1.071	1.275	1.375	1.480	1.593	1.715	1.928	2.123	2.334	2.520	2.614	2.672	2.641	2.518	1.655
19.81	1.000	1.163	1.344	1.431	1.521	1.613	1.722	1.921	2.077	2.248	2.391	2.447	2.476	2.427	2.281	1.659
24.83	1.098	1.244	1.414	1.491	1.567	1.651	1.745	1.910	2.042	2.185	2.304	2.330	2.334	2.279	2.122	1.670
29.87	1.164	1.299	1.452	1.519	1.588	1.658	1.745	1.882	1.991	2.105	2.200	2.211	2.199	2.138	1.987	1.692
34.73	1.227	1.349	1.494	1.550	1.616	1.675	1.753	1.879	1.968	2.067	2.144	2.136	2.103	2.029	1.904	1.703
39.96	1.294	1.406	1.539	1.591	1.648	1.703	1.774	1.879	1.954	2.040	2.099	2.078	2.028	1.944	1.864	1.709
45.00	1.339	1.439	1.559	1.609	1.658	1.709	1.767	1.850	1.908	1.990	2.017	1.986	1.907	1.830	1.784	1.723
50.08	1.406	1.495	1.604	1.651	1.693	1.737	1.795	1.871	1.912	1.962	1.989	1.944	1.829	1.738	1.798	1.756
55.12	1.326	1.411	1.513	1.578	1.606	1.648	1.631	1.707	1.723	1.758	1.774	1.725	1.612	1.562	1.762	1.760
60.15	1.217	1.266	1.343	1.375	1.427	1.432	1.480	1.537	1.510	1.577	1.583	1.542	1.462	1.484	1.747	1.760
65.15	1.137	1.182	1.244	1.269	1.287	1.310	1.347	1.391	1.397	1.415	1.413	1.388	1.398	1.467	1.733	1.760
70.15	1.053	1.094	1.141	1.162	1.179	1.194	1.225	1.259	1.259	1.243	1.277	1.282	1.370	1.463	1.715	1.749
80.08	0.909	0.932	0.961	0.973	0.983	0.992	1.011	1.050	1.056	1.082	1.121	1.175	1.334	1.439	1.660	1.726
90.02	0.797	0.808	0.822	0.829	0.832	0.838	0.854	0.904	0.923	0.992	1.048	1.115	1.288	1.368	1.555	1.681
								Lower Surface								
0.63	3.230	2.059	1.215	0.854	0.667	0.326	0.164	-0.016	0.026	0.217	0.487	0.868	1.151	1.467	1.527	0.195
0.90	3.138	2.081	1.297	0.956	0.680	0.400	0.257	0.027	0	0.073	0.238	0.502	0.701	0.857	0.982	0.084
1.41	2.961	2.081	1.389	1.070	0.833	0.595	0.411	0.123	0.016	-0.010	0.031	0.167	0.272	0.372	0.449	-0.011
2.69	2.672	1.996	1.461	1.211	0.997	0.792	0.617	0.336	0.161	+0.052	0	0.005	0.021	0.041	0.075	-0.006
5.20	2.205	1.799	1.399	1.232	1.063	0.927	0.781	0.539	0.368	0.217	0.124	0.066	0.031	0.021	0.022	0.084
7.73	1.997	1.670	1.383	1.239	1.106	0.969	0.836	0.649	0.481	0.347	0.243	0.164	0.117	0.077	0.084	0.174
10.23	1.871	1.578	1.366	1.239	1.123	1.004	0.910	0.718	0.552	0.433	0.330	0.253	0.199	0.155	0.156	0.259
15.21	1.759	1.539	1.348	1.246	1.154	1.057	0.976	0.815	0.677	0.565	0.466	0.390	0.334	0.285	0.287	0.379
20.19	1.689	1.504	1.355	1.253	1.182	1.098	1.022	0.890	0.761	0.662	0.570	0.499	0.445	0.398	0.400	0.484
25.17	1.644	1.486	1.359	1.280	1.211	1.133	1.074	0.953	0.831	0.741	0.656	0.591	0.537	0.497	0.501	0.524
30.13	1.619	1.480	1.366	1.295	1.221	1.162	1.109	1.000	0.884	0.803	0.723	0.663	0.616	0.578	0.585	0.653
35.08	1.594	1.472	1.376	1.312	1.253	1.193	1.144	1.042	0.937	0.862	0.785	0.731	0.687	0.655	0.668	0.728
40.04	1.606	1.493	1.400	1.344	1.287	1.231	1.190	1.096	0.993	0.928	0.858	0.803	0.676	0.736	0.759	0.814
45.00	1.606	1.502	1.413	1.368	1.308	1.258	1.221	1.142	1.042	0.982	0.923	0.871	0.836	0.826	0.839	0.916
49.92	1.588	1.496	1.438	1.382	1.329	1.282	1.249	1.181	1.088	1.034	0.982	0.936	0.904	0.900	0.923	1.003
54.88	1.459	1.393	1.339	1.315	1.266	1.222	1.193	1.132	1.049	1.003	0.961	0.923	0.900	0.903	0.930	1.006
59.85	1.343	1.277	1.225	1.179	1.133	1.107	1.109	1.067	1.000	0.957	0.919	0.893	0.879	0.886	0.919	0.991
64.85	1.238	1.185	1.155	1.109	1.071	1.041	1.025	0.992	0.929	0.912	0.891	0.871	0.861	0.872	0.912	0.984
69.88	1.151	1.104	1.065	1.043	1.015	0.988	0.980	0.950	0.898	0.885	0.864	0.871	0.850	0.868	0.916	0.987
79.92	0.989	0.956	0.933	0.917	0.896	0.877	0.875	0.857	0.821	0.816	0.811	0.813	0.825	0.847	0.908	0.987
89.99	0.874	0.847	0.825	0.812	0.798	0.789	0.788	0.783	0.761	0.771	0.780	0.789	0.825	0.861	0.937	1.036

* These data are uncorrected for tunnel wall effect.

TABLE VII - EXPERIMENTAL VALUES OF $\left(\frac{v}{V_o}\right)^2$ FOR JUNCTION OF NACA 35-215 WING-*

NACA 133-30 NACELLE UNIT

Reynolds Number = 5.75×10^6 Mach Number = 0.20

C_{l_w} / α / %c	-0.448	-0.217	+0.012	0.138	0.243	0.357	0.478	0.688	0.879	1.060	1.220	1.305	1.386	1.418	1.428	0.670
	-5°	-3°	-1°	0°	1°	2°	3°	5°	7°	9°	11°	13°	15°	17°	19°	20°
							Upper Surface									
0	0.398	0.133	0	0.079	-0.010	0.030	0.123	0.347	0.711	1.144	1.619	2.180	2.690	2.911	2.871	1.792
0.38	0.031	0	0.070	0.147	0.258	0.421	0.592	1.073	1.663	2.114	2.692	3.409	4.015	4.238	4.120	2.201
0.60	0.010	0.020	0.140	0.236	0.367	0.521	0.715	1.256	1.653	2.135	2.732	3.430	3.994	4.218	4.090	2.191
1.08	0.010	0.082	0.240	0.354	0.506	0.661	0.878	1.359	1.643	2.217	2.742	3.337	3.816	3.972	3.845	2.181
2.31	0.112	0.255	0.461	0.560	0.735	0.912	1.082	1.399	1.833	2.298	2.722	3.192	3.566	3.677	3.559	2.064
4.79	0.317	0.491	0.712	0.820	0.994	1.143	1.238	1.614	1.927	2.310	2.707	3.080	3.365	3.433	3.305	2.020
7.27	0.477	0.657	0.873	0.973	1.118	1.229	1.369	1.662	1.974	2.314	2.648	2.978	3.234	3.262	3.128	1.982
9.77	0.609	0.788	0.996	1.098	1.226	1.359	1.482	1.745	2.029	2.310	2.624	2.908	3.180	3.201	3.063	1.951
14.79	0.808	0.979	1.170	1.251	1.367	1.489	1.598	1.821	2.060	2.296	2.551	2.802	2.973	2.862	2.691	1.931
19.81	0.882	1.127	1.304	1.380	1.485	1.595	1.693	1.886	2.094	2.279	2.513	2.664	2.752	2.658	2.435	1.934
24.83	1.103	1.262	1.417	1.489	1.586	1.688	1.778	1.945	2.131	2.282	2.478	2.565	2.610	2.497	2.261	1.944
29.87	1.225	1.369	1.516	1.581	1.671	1.763	1.845	1.996	2.155	2.286	2.439	2.481	2.496	2.379	2.128	1.948
34.73	1.337	1.473	1.619	1.683	1.762	1.849	1.926	2.061	2.199	2.303	2.422	2.382	2.396	2.309	2.056	1.968
39.96	1.438	1.566	1.704	1.768	1.839	1.921	1.990	2.099	2.210	2.275	2.391	2.241	2.232	2.232	1.941	1.934
45.00	1.556	1.684	1.814	1.874	1.933	2.006	2.071	2.157	2.251	2.286	2.363	2.071	2.061	2.104	1.879	1.948
50.08	1.643	1.763	1.879	1.931	1.989	2.054	2.106	2.157	2.213	2.214	2.245	1.782	1.815	1.966	1.825	1.962
55.12	1.580	1.684	1.786	1.829	1.869	1.921	1.965	1.968	1.991	1.950	1.917	1.683	1.715	1.805	1.787	1.968
60.15	1.493	1.577	1.660	1.692	1.724	1.760	1.788	1.745	1.698	1.679	1.688	1.662	1.693	1.718	1.753	1.965
65.15	1.396	1.466	1.530	1.551	1.570	1.585	1.609	1.642	1.616	1.554	1.628	1.620	1.636	1.671	1.743	1.958
70.15	1.302	1.362	1.410	1.425	1.442	1.465	1.506	1.570	1.545	1.474	1.555	1.591	1.594	1.638	1.733	1.944
80.08	1.124	1.158	1.225	1.244	1.266	1.301	1.330	1.364	1.391	1.384	1.451	1.528	1.512	1.591	1.729	1.910
90.02	0.995	1.013	1.061	1.078	1.088	1.113	1.129	1.141	1.190	1.266	1.347	1.411	1.447	1.560	1.722	1.876
							Lower Surface									
0.63	0.899	0.613	0.311	0.197	0.099	0.050	0.020	-0.010	0.060	0.204	0.415	0.671	0.959	1.023	1.042	1.626
0.90	1.410	0.827	0.471	0.324	0.189	0.130	0.060	0	0.030	0.143	0.283	0.465	0.709	0.777	0.816	1.461
1.41	1.491	0.981	0.601	0.452	0.318	0.230	0.143	0.031	0	0.051	0.121	0.227	0.396	0.433	0.472	0.273
2.69	1.491	1.144	0.812	0.639	0.506	0.411	0.306	0.143	0.040	0.010	0.010	0.031	0.104	0.098	0.138	0.088
5.20	1.593	1.256	1.012	0.865	0.715	0.621	0.521	0.337	0.190	0.112	0.051	0.021	0.020	0	0.030	0.068
7.73	1.653	1.342	1.109	0.993	0.852	0.757	0.656	0.481	0.327	0.225	0.143	0.081	0.060	0.045	0.044	0.103
10.23	1.678	1.398	1.184	1.068	0.946	0.856	0.758	0.587	0.429	0.323	0.233	0.159	0.128	0.101	0.109	0.189
15.21	1.723	1.487	1.300	1.190	1.085	1.003	0.913	0.749	0.596	0.486	0.390	0.311	0.264	0.238	0.249	0.347
20.19	1.761	1.556	1.386	1.289	1.189	1.113	1.033	0.879	0.726	0.617	0.529	0.448	0.403	0.379	0.399	0.502
25.17	1.793	1.608	1.458	1.367	1.277	1.208	1.136	0.987	0.852	0.739	0.651	0.575	0.520	0.510	0.529	0.642
30.13	1.824	1.656	1.525	1.438	1.354	1.291	1.227	1.086	0.954	0.844	0.759	0.688	0.635	0.634	0.655	0.780
35.08	1.862	1.708	1.588	1.513	1.431	1.369	1.316	1.178	1.050	0.950	0.867	0.794	0.745	0.755	0.784	0.914
40.04	1.890	1.753	1.639	1.574	1.495	1.441	1.393	1.264	1.139	1.041	0.964	0.900	0.856	0.876	0.914	1.055
45.00	1.911	1.795	1.694	1.632	1.563	1.513	1.464	1.340	1.224	1.113	1.075	0.981	0.945	0.990	1.027	1.151
49.92	1.911	1.812	1.728	1.676	1.613	1.565	1.524	1.408	1.296	1.190	1.159	1.076	1.045	1.104	1.146	1.285
54.88	1.796	1.719	1.653	1.608	1.553	1.510	1.467	1.367	1.275	1.183	1.162	1.090	1.066	1.134	1.190	1.319
59.85	1.650	1.587	1.533	1.496	1.452	1.414	1.376	1.285	1.214	1.137	1.127	1.066	1.052	1.124	1.187	1.316
64.85	1.521	1.476	1.431	1.401	1.361	1.332	1.298	1.226	1.163	1.094	1.103	1.048	1.037	1.121	1.190	1.316
69.88	1.410	1.373	1.335	1.312	1.280	1.253	1.227	1.165	1.118	1.061	1.072	1.027	1.027	1.117	1.190	1.312
79.92	1.222	1.189	1.160	1.142	1.118	1.096	1.076	1.037	1.006	0.970	0.992	0.963	0.977	1.081	1.170	1.285
89.99	1.079	1.051	1.030	1.017	0.997	0.986	0.970	0.952	0.935	0.914	0.964	0.949	0.984	1.094	1.197	1.326

* These data are uncorrected for tunnel wall effects.

TABLE VIII - EXPERIMENTAL VALUES OF $\left(\frac{V}{V_o}\right)^2$ FOR TOP AND BOTTOM NACELLE MERIDIAN OF NACA 35-215 WING-NACA 133-30 NACELLE UNIT *

Reynolds Number = 5.75×10^6 Mach Number = 0.20

C_{l_w} / α / x/c	-0.448	-0.217	+0.012	0.138	0.243	0.357	0.478	0.688	0.879	1.060	1.220	1.305	1.386	1.418	1.428	0.670
	-5°	-3°	-1°	0°	1°	2°	3°	5°	7°	9°	11°	13°	15°	17°	19°	20°
							Upper Surface									
0	0.398	0.133	0	0.079	-0.010	0.030	0.123	0.347	0.711	1.144	1.619	2.180	2.690	2.911	2.871	1.792
1.25	0.061	0.184	0.361	0.472	0.606	0.752	0.919	1.277	1.673	2.074	2.489	2.944	3.326	3.471	4.366	2.541
2.50	0.255	0.419	0.621	0.737	0.884	1.022	1.184	1.512	1.863	2.196	2.540	2.924	3.222	3.333	4.108	2.347
5.00	0.460	0.654	0.852	0.964	1.092	1.222	1.358	1.634	1.923	2.186	2.459	2.717	2.899	2.979	2.861	2.191
7.50	0.675	0.851	1.051	1.156	1.263	1.380	1.503	1.730	1.981	2.199	2.460	2.639	2.791	2.856	2.742	2.116
10.00	0.787	0.947	1.146	1.244	1.344	1.455	1.559	1.759	1.978	2.161	2.478	2.512	2.631	2.799	2.681	2.113
15.00	0.961	1.110	1.287	1.374	1.456	1.558	1.644	1.803	1.984	2.161	2.339	2.385	2.463	2.557	2.432	2.099
20.00	1.096	1.231	1.389	1.455	1.522	1.602	1.686	1.817	2.002	2.112	2.262	2.276	2.328	2.417	2.299	2.099
25.00	1.211	1.335	1.480	1.547	1.607	1.681	1.753	1.862	1.981	2.067	2.192	2.223	2.253	2.312	2.203	2.113
30.00	1.288	1.400	1.520	1.581	1.637	1.701	1.764	1.848	1.947	1.979	2.112	2.128	2.153	2.211	2.108	2.113
35.00	1.319	1.418	1.520	1.578	1.617	1.678	1.729	1.782	1.872	1.918	1.997	1.994	2.000	2.077	1.985	2.109
40.00	1.316	1.404	1.489	1.530	1.559	1.615	1.633	1.687	1.756	1.752	1.844	1.849	1.847	1.919	1.859	2.120
50.00	1.239	1.293	1.359	1.384	1.404	1.439	1.467	1.491	1.527	1.533	1.580	1.567	1.558	1.651	1.712	2.161
60.00	1.145	1.186	1.222	1.238	1.243	1.270	1.280	1.288	1.306	1.304	1.333	1.330	1.358	1.453	1.692	2.133
70.00	1.089	1.105	1.135	1.132	1.135	1.145	1.153	1.140	1.135	1.110	1.127	1.154	1.234	1.322	1.630	2.068
80.00	1.069	1.072	1.075	1.071	1.060	1.071	1.062	1.024	0.999	0.971	1.016	1.083	1.141	1.248	1.480	1.996
							Lower Surface									
1.25	1.297	0.940	0.631	0.501	0.377	0.281	0.204	0.061	-0.010	-0.020	0	0.052	0.146	0.157	0.187	0.146
5.00	1.614	1.359	1.092	0.973	0.864	0.762	0.664	0.480	0.341	0.235	0.152	0.093	0.062	0.029	0.059	0.107
10.00	1.671	1.459	1.277	1.187	1.088	1.003	0.920	0.752	0.610	0.503	0.418	0.325	0.278	0.248	0.256	0.330
20.00	1.737	1.587	1.475	1.387	1.310	1.243	1.182	1.041	0.920	0.819	0.745	0.660	0.613	0.597	0.628	0.715
30.00	1.726	1.615	1.530	1.479	1.421	1.369	1.316	1.199	1.108	1.013	0.961	0.889	0.856	0.862	0.907	1.013
40.00	1.594	1.525	1.482	1.442	1.397	1.361	1.323	1.233	1.163	1.089	1.061	1.016	0.998	1.020	1.091	1.220

* These data are uncorrected for tunnel wall effect.

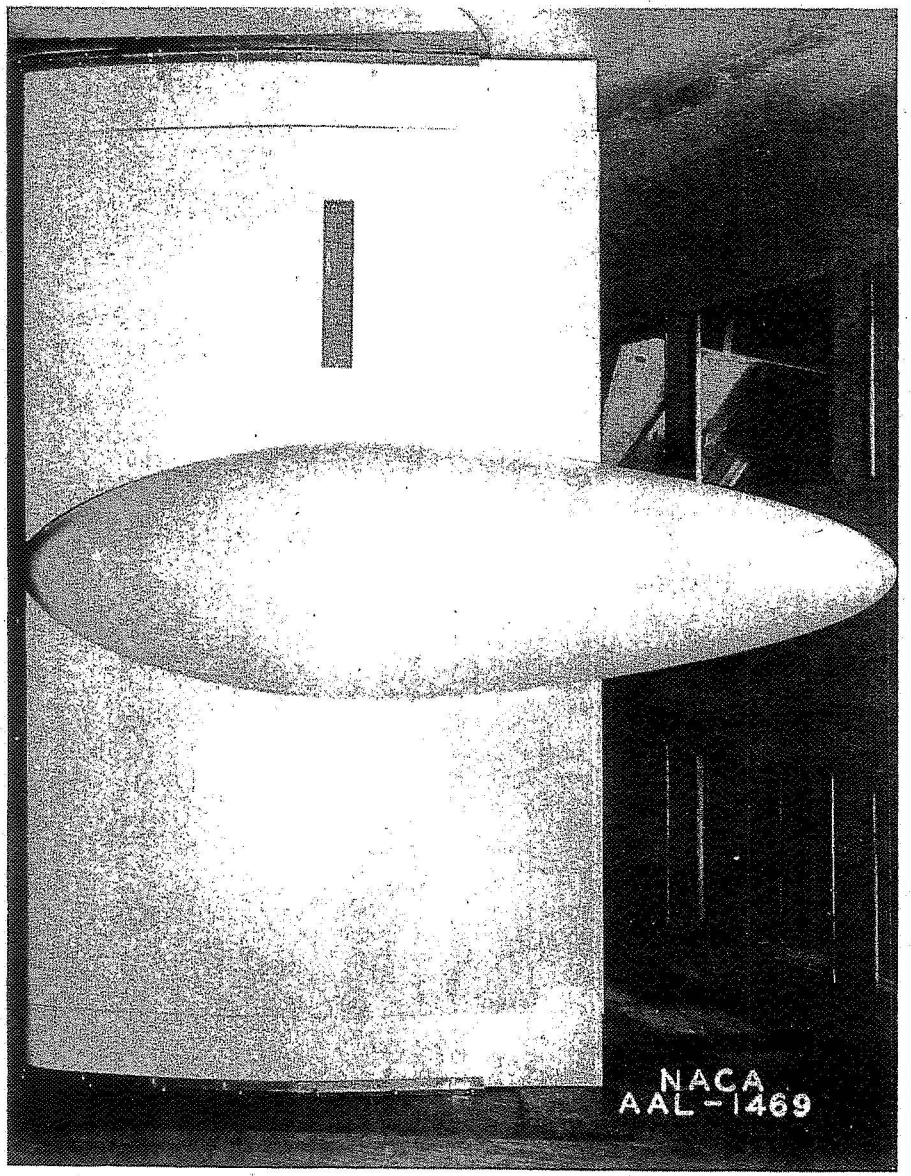

Figure 1.- Lower surface of wing-nacelle (NACA 133-30)

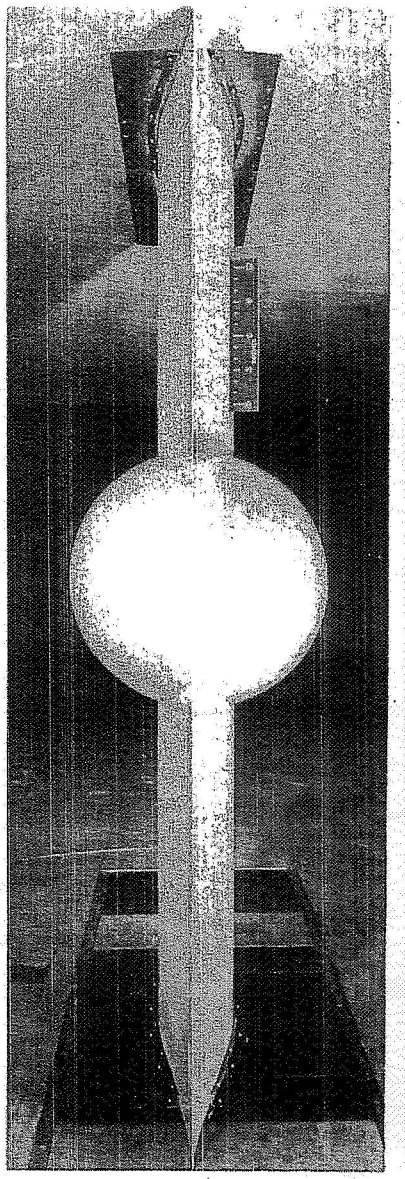

Figure 2.- Rear view of wing-nacelle (NACA 133-30)

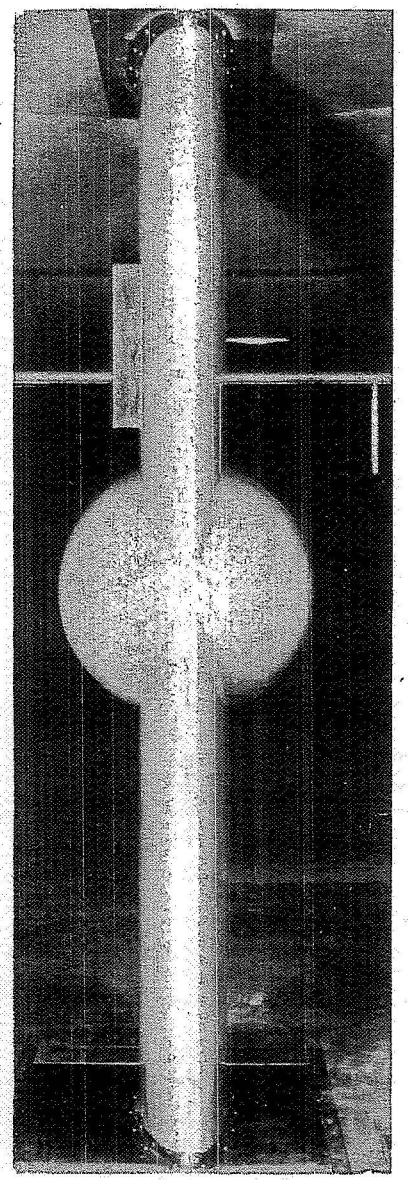

Figure 3.- Front view of wing-nacelle NACA 133-30 (wing-nacelle NACA 230-38 similar).

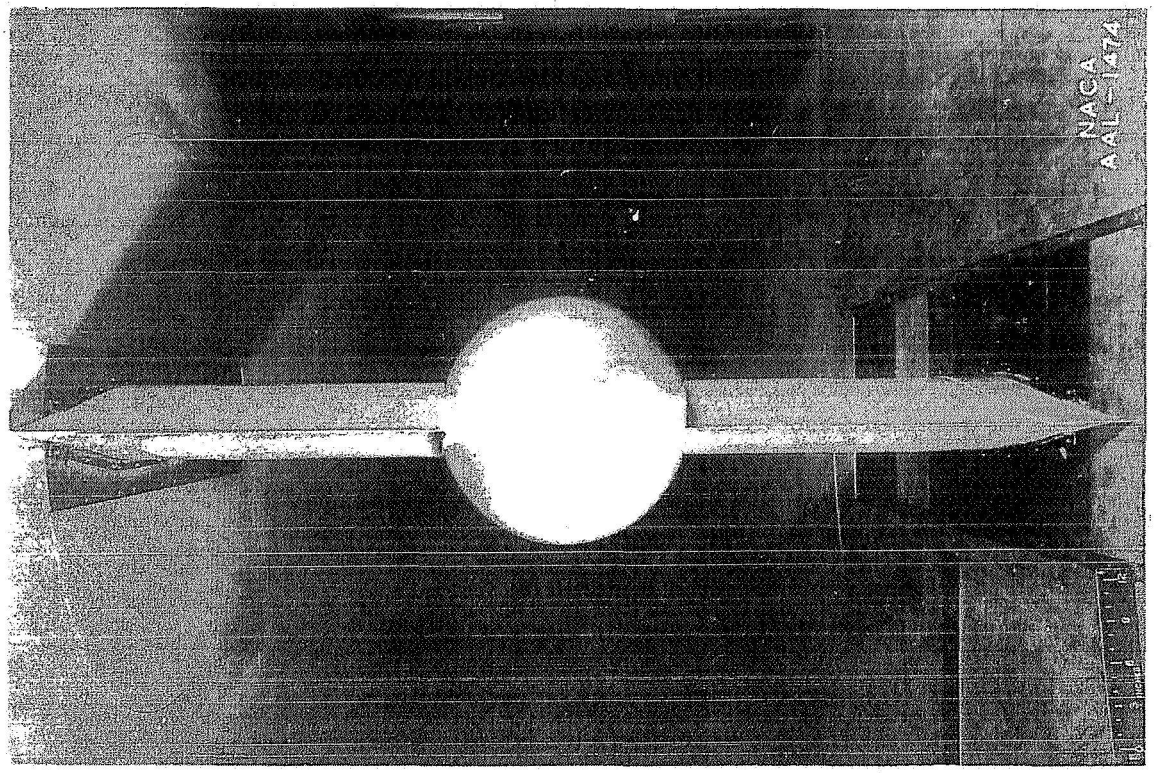

Figure 5.- Rear view of wing nacelle (NACA 230-28).

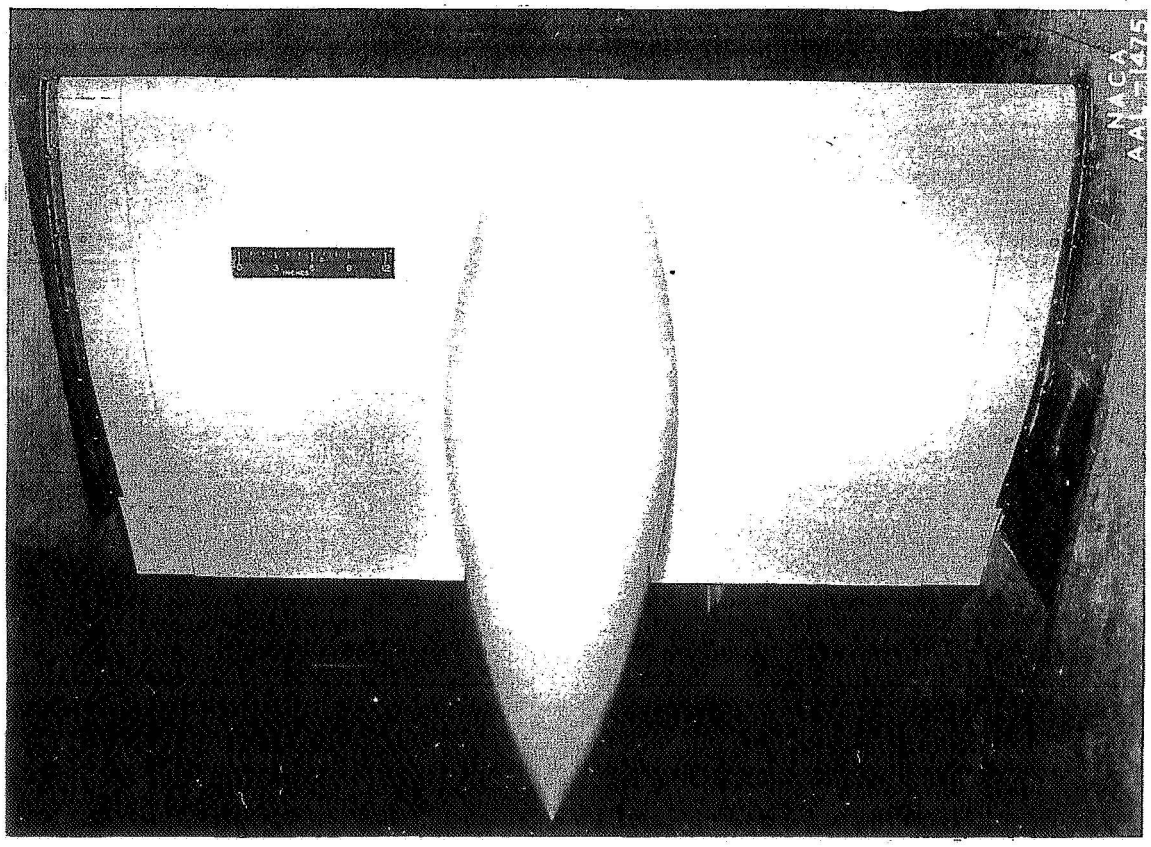

Figure 4.- Upper surface of wing nacelle (NACA 230-28).

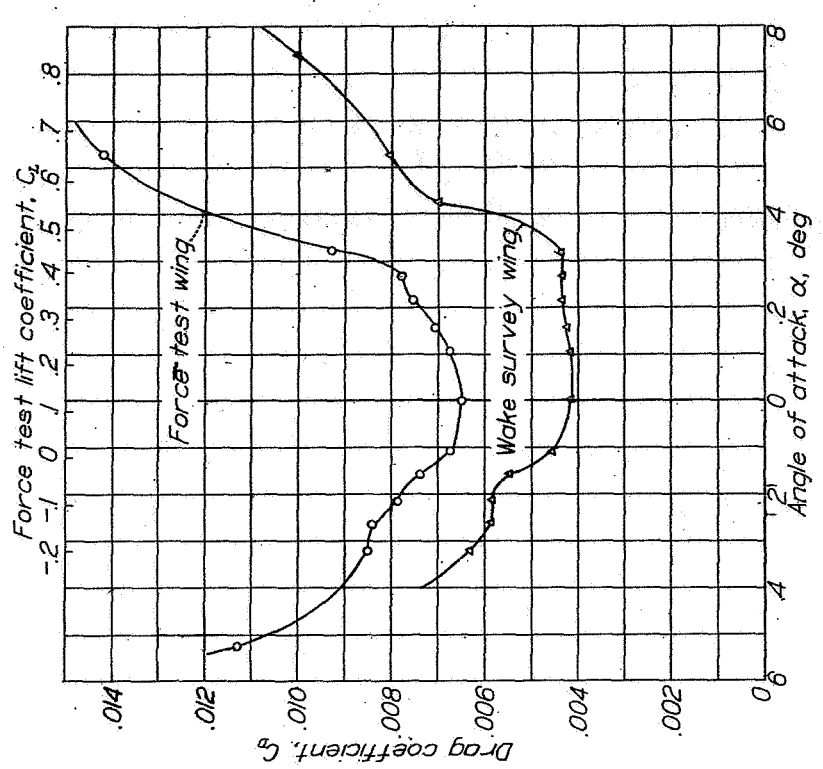

Figure 7.- Section and force test drag coefficient variation with angle of attack for NACA 35-215 wing. Reynolds number 5,750,000.

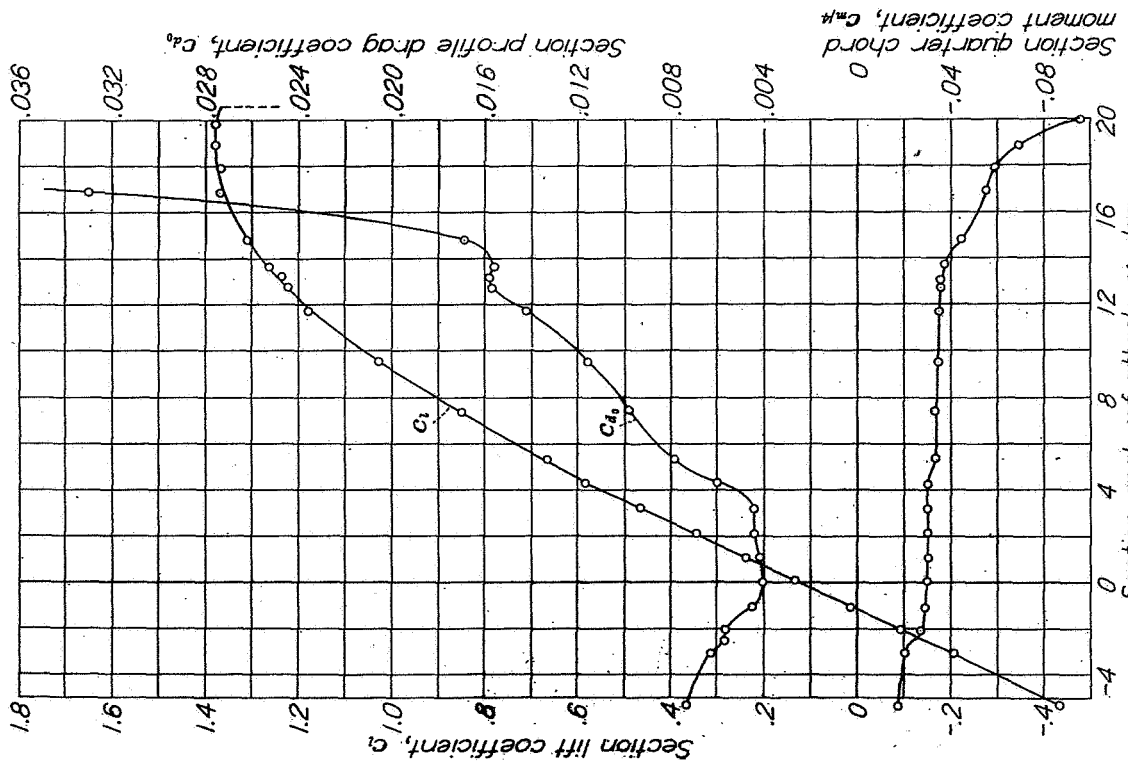

Figure 6.- Characteristics of the NACA 35-215 wing profile as determined by pressure distribution and wake measurements. Mach number = 0.20. Reynolds number = 5,750,000.

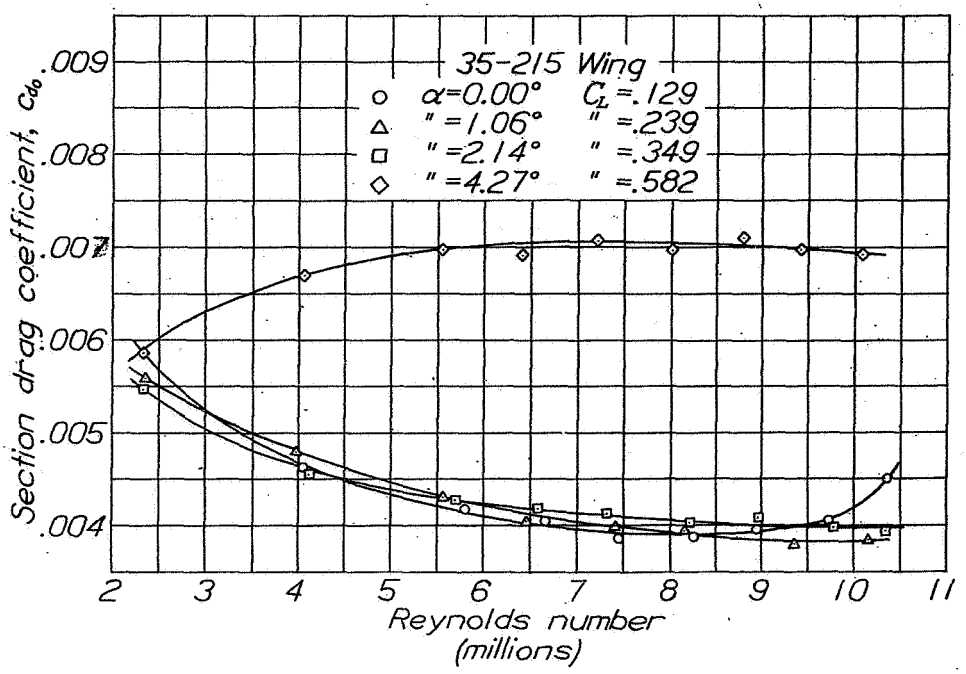

Figure 8.- Section drag coefficient variation with Reynolds number for NACA 35-215 wing.

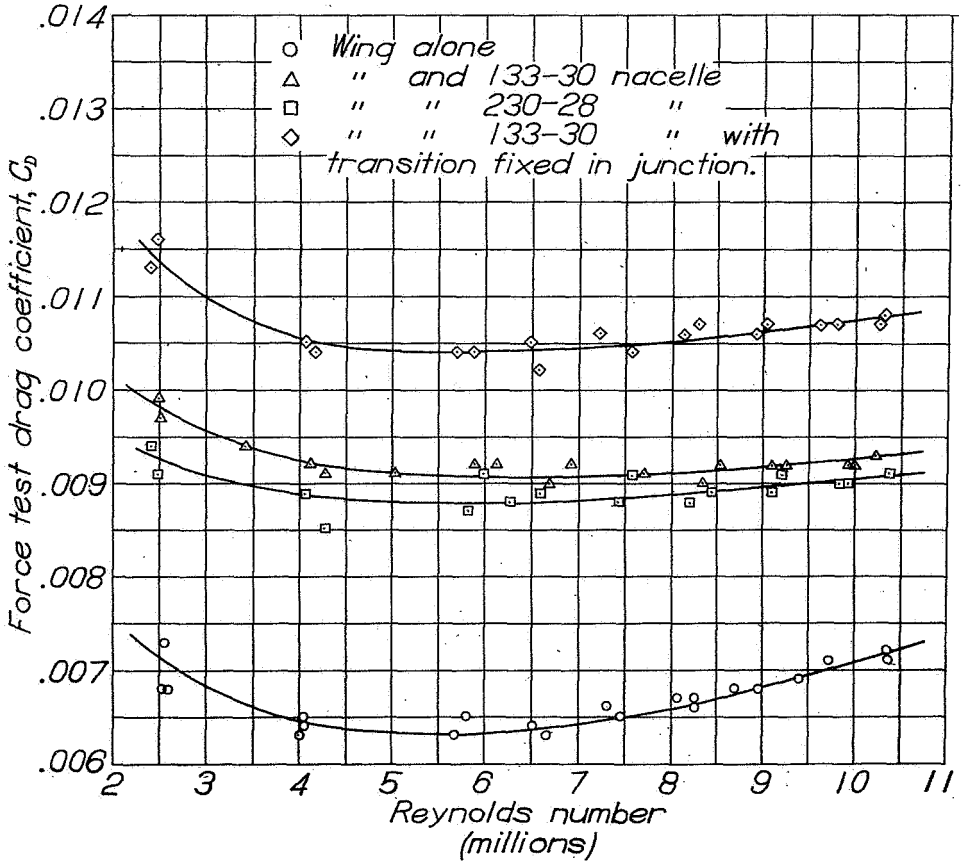

Figure 9.- Force test drag coefficient variation with Reynolds number $\alpha = 0^o$. $C_L = .120$.

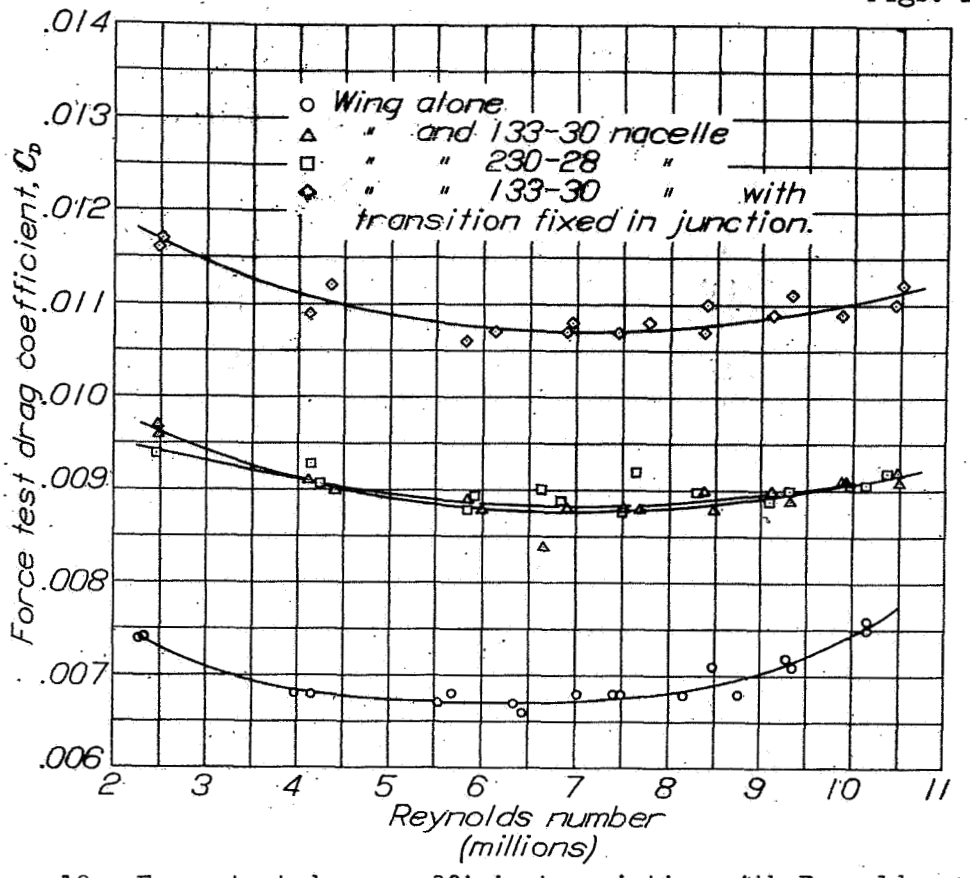

Figure 10.- Force test drag coefficient variation with Reynolds number $\alpha = 1.06^{\circ}$, $C_L = .233$.

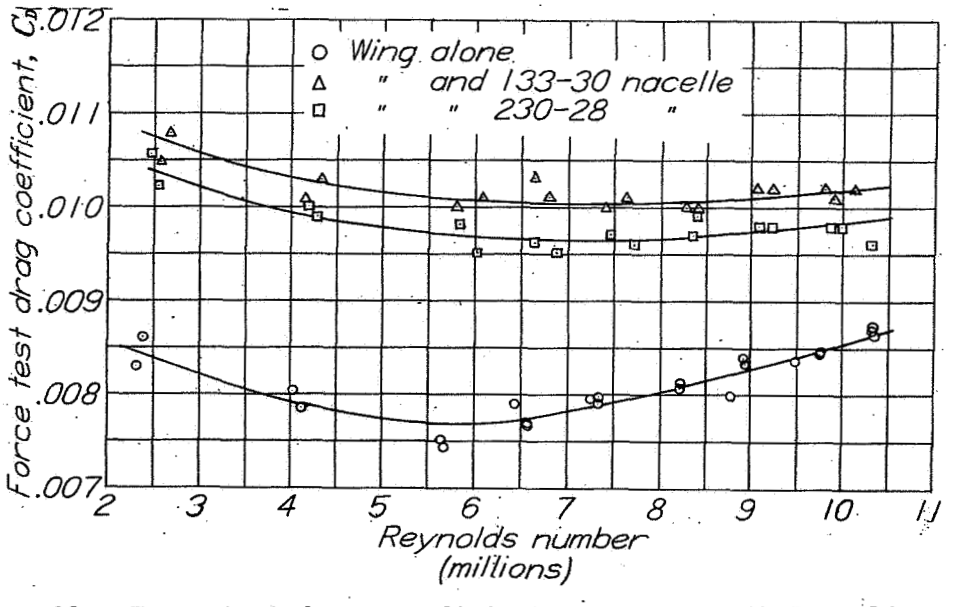

Figure 11.- Force test drag coefficient variation with Reynolds number $\alpha = 2.14^{\circ}$, $C_L = .335$.

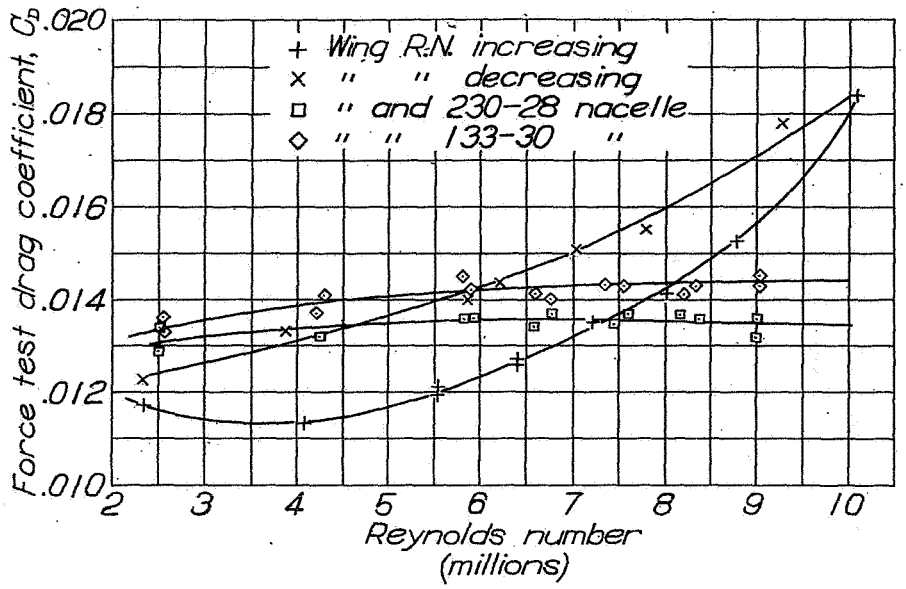

Figure 12.- Force test drag coefficient variation with Reynolds number $\alpha = 4.27^\circ$, $C_L = .565$.

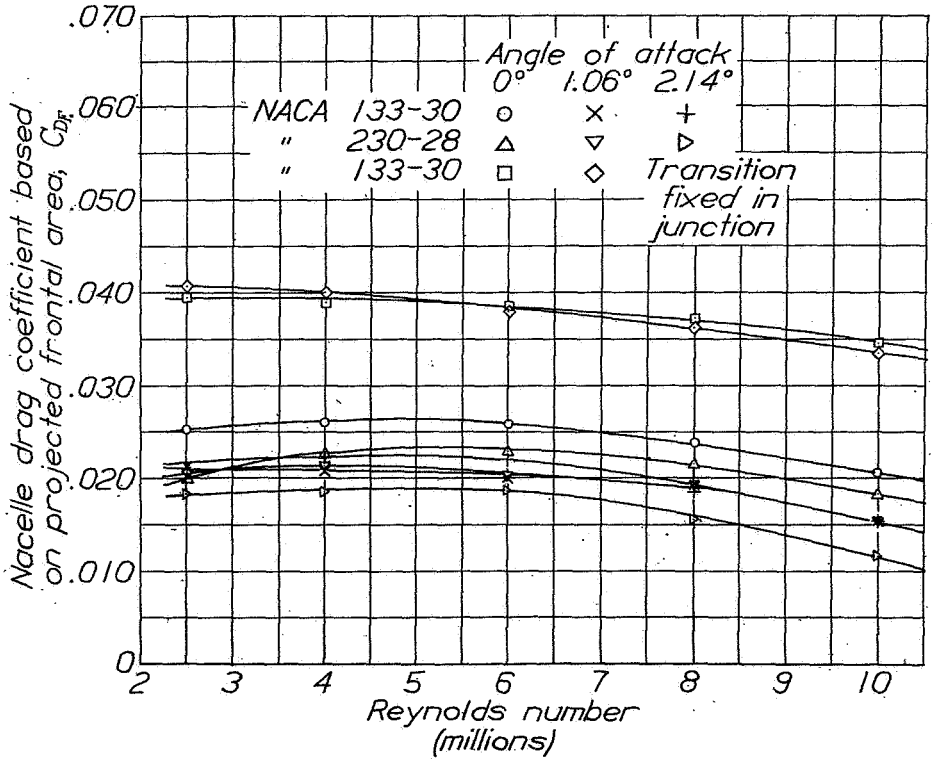

Figure 13.- Variation of nacelle drag coefficient based on projected frontal area with Reynolds number.

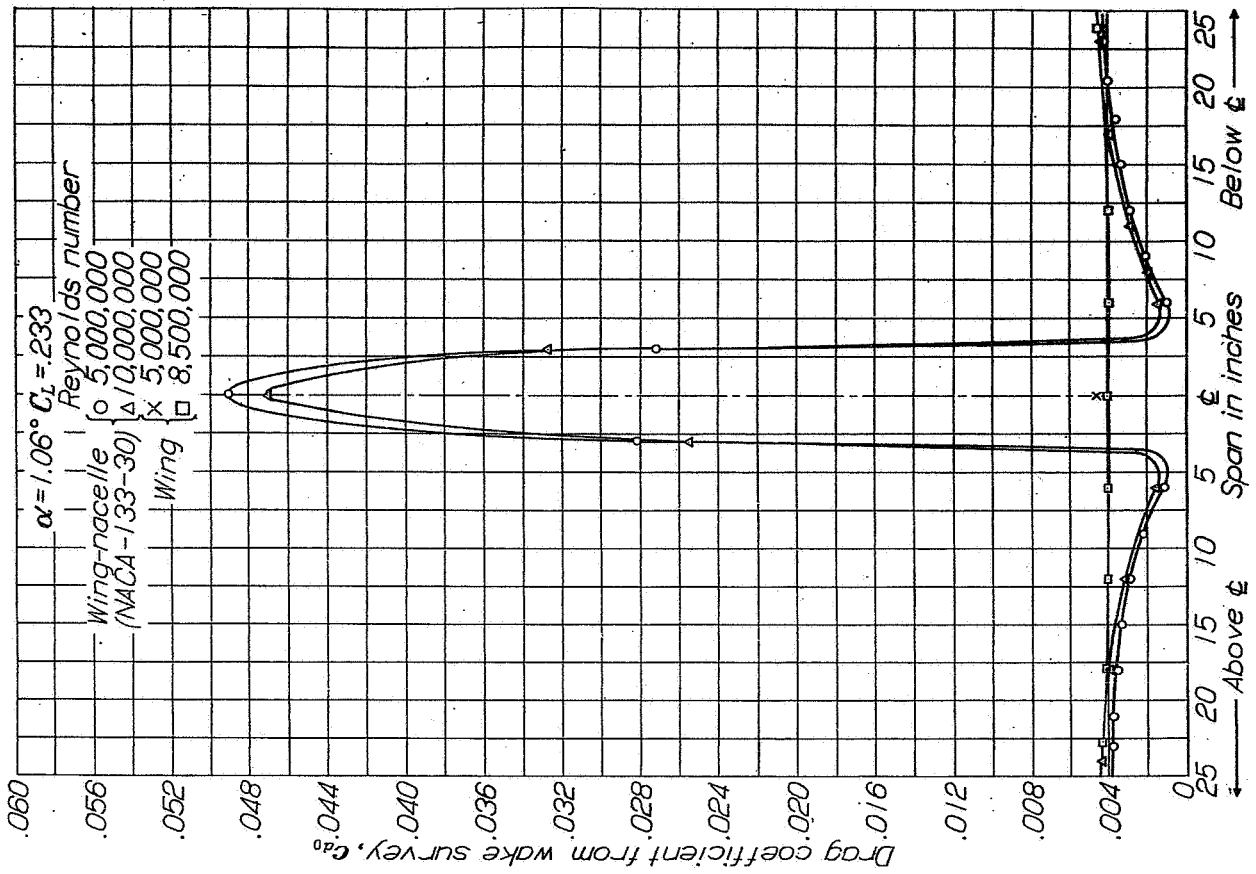

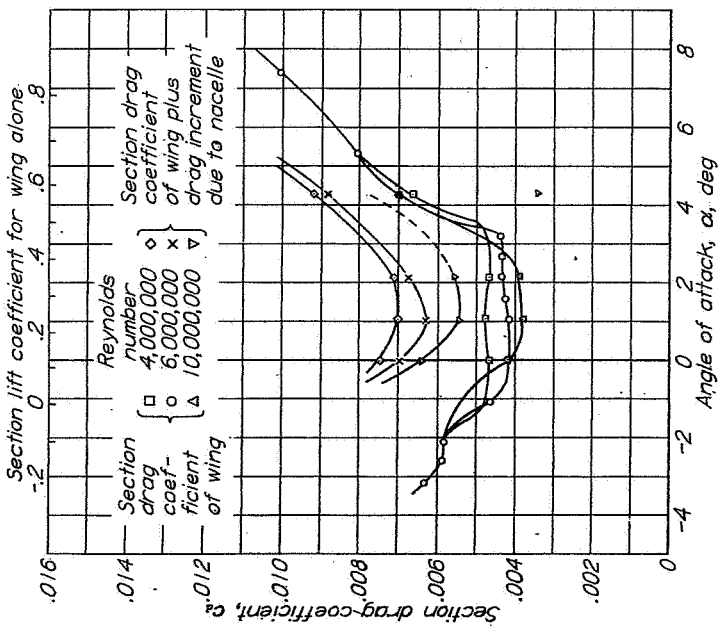

Figure 14.- Drag coefficient variation with angle of attack for NACA 35-215 wing and NACA 35-215 wing-NACA 133-30 nacelle combination.

Figure 15.- (right) Spanwise variation of drag coefficient base on wing chord as determined by wake surveys. Total span 72 inches.

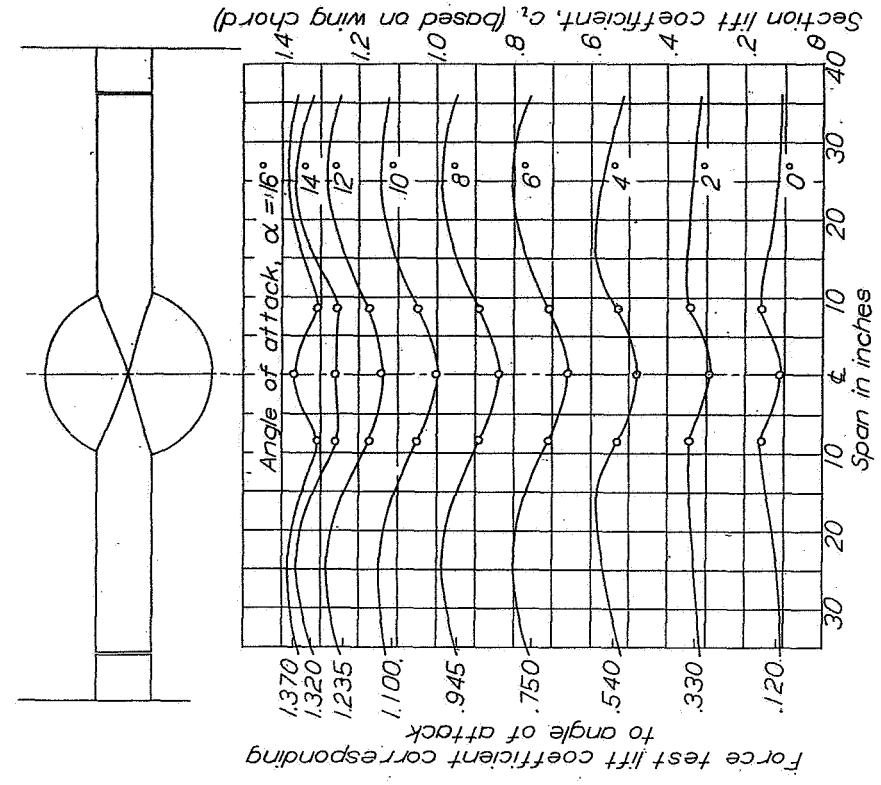

Figure 17.- Spanwise variation of section lift coefficient wing-nacelle (NACA 133-30). Reynolds number = 5,750,000. Mach number = 0.20.

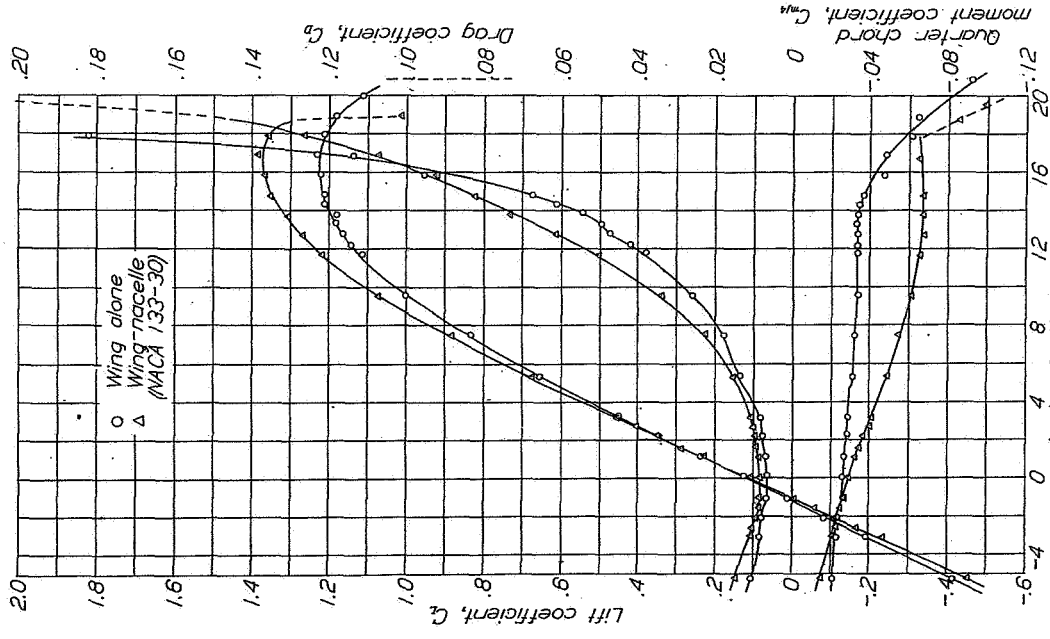

Figure 16.- Characteristics of wing and of wing-nacelle (NACA 133-30) combination as determined by balance force measurement. Reynolds number = 3,250,000. Mach number = 0.20.

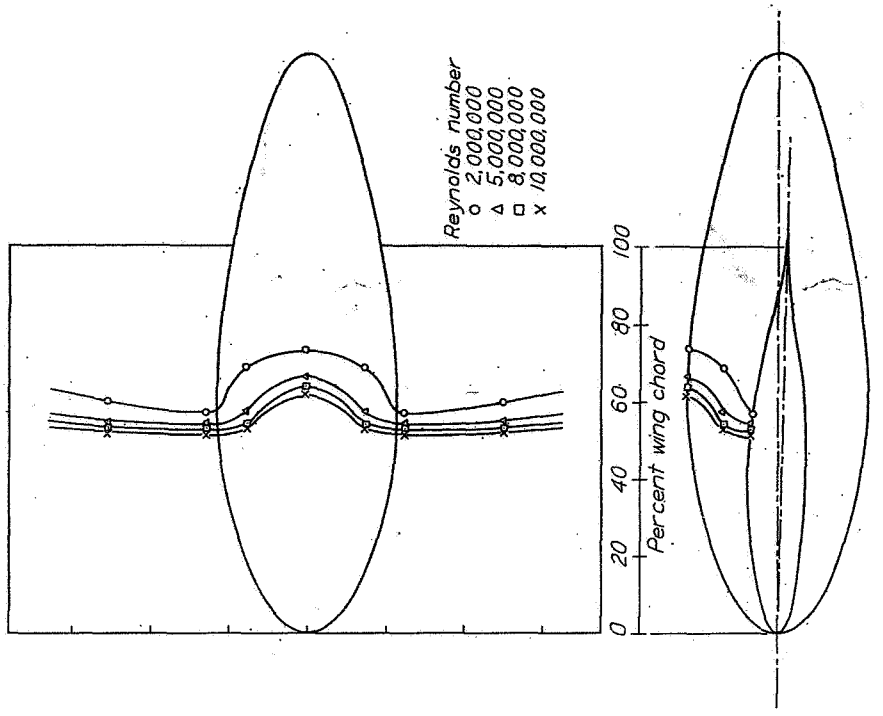

Figure 19.- Spanwise location of transition for various Reynolds numbers $\alpha = 0^{\circ}$, $C_L = .120$. Upper surface wing-nacelle (NACA 133-30).

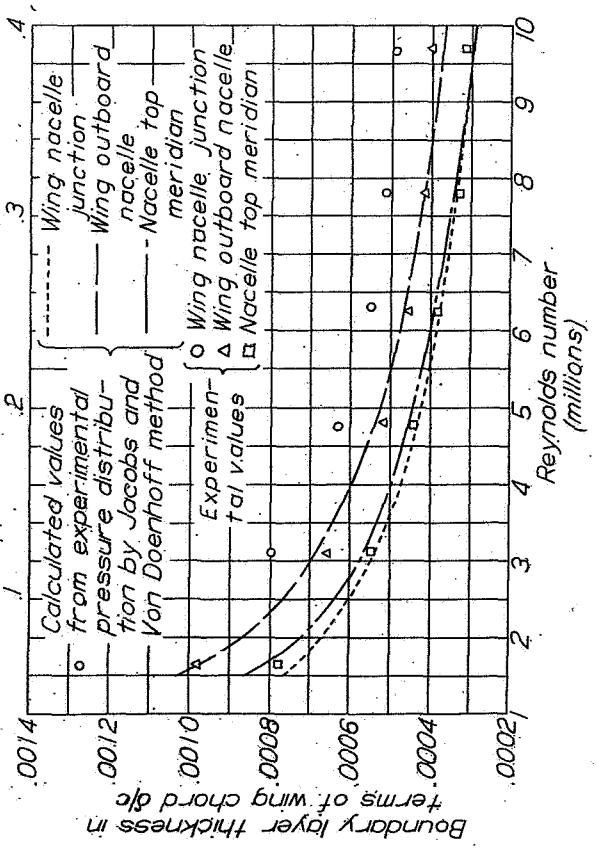

Figure 18.- Variation of boundary-layer thickness with Reynolds number at $\alpha = 1.06^{\circ}$, $C_L = .233$ for wing and nacelle (NACA 133-30).

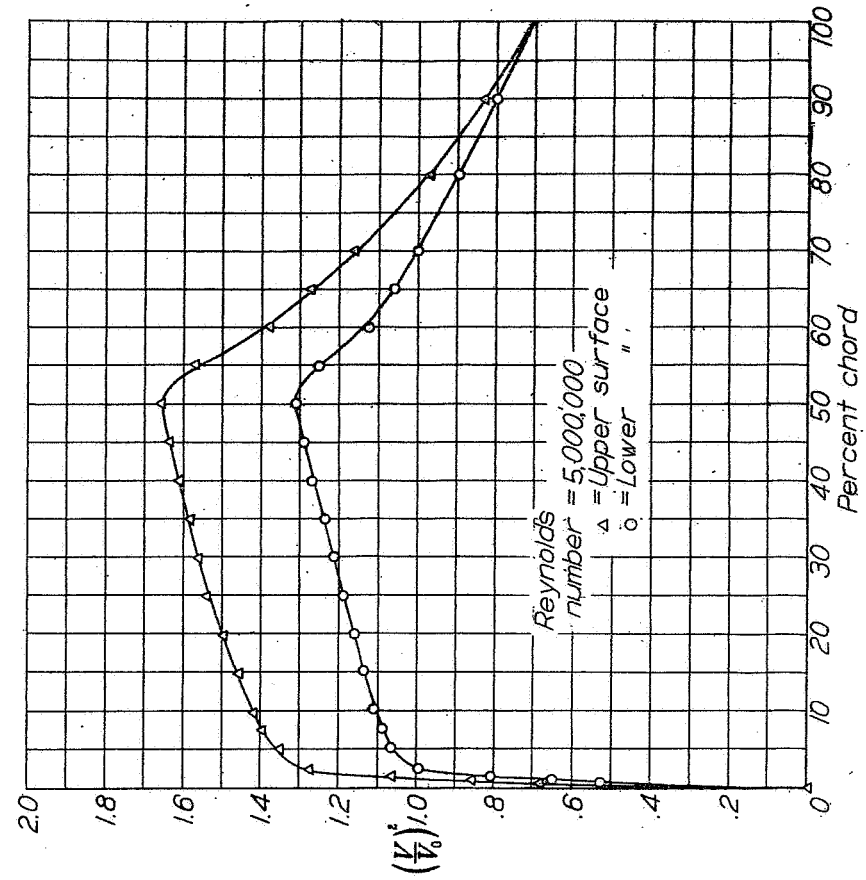

Figure 21.- Experimental pressure distribution for wing at design lift coefficient. NACA 35-215 wing, $\alpha = 1.00$, $C_L = .24$. Corrected to Mach number = 0. Uncorrected for tunnel wall effects except constriction.

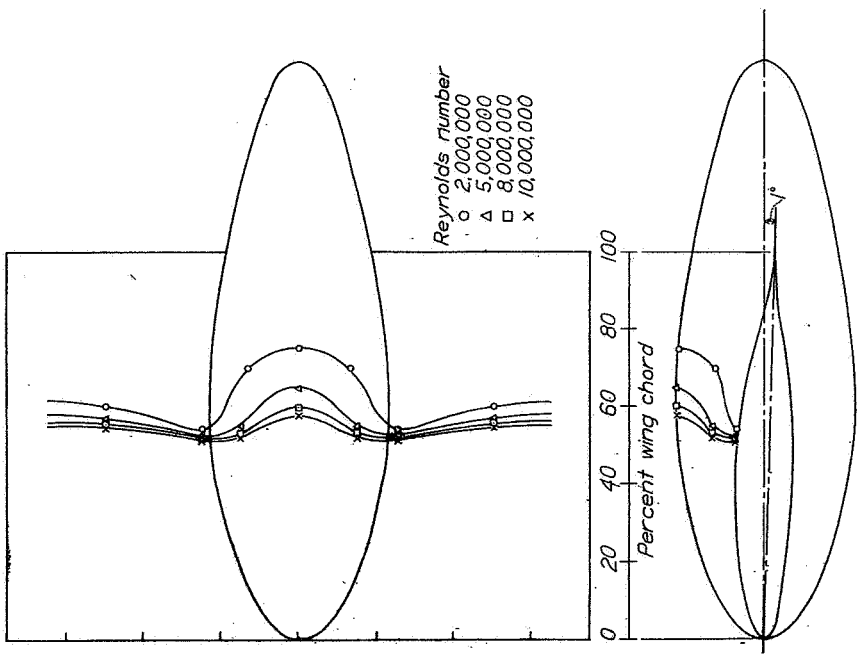

Figure 20.- Spanwise location of transition for various Reynolds numbers $\alpha = 1.06°$, $C_L = .233$. Upper surface, wing-nacelle (NACA 133-30).

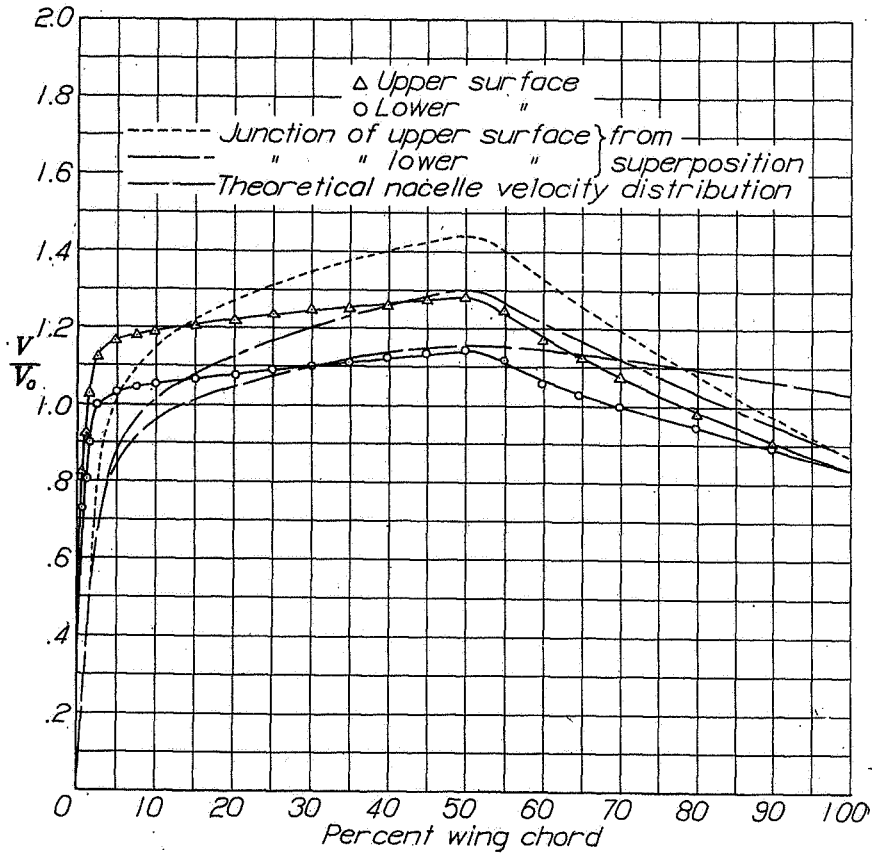

Figure 22.- Superposition of velocities in the wing-nacelle (NACA 133-30) junction. Experimental wing velocity distribution corrected to Mach number = 0, Reynolds number = 5,000,000.

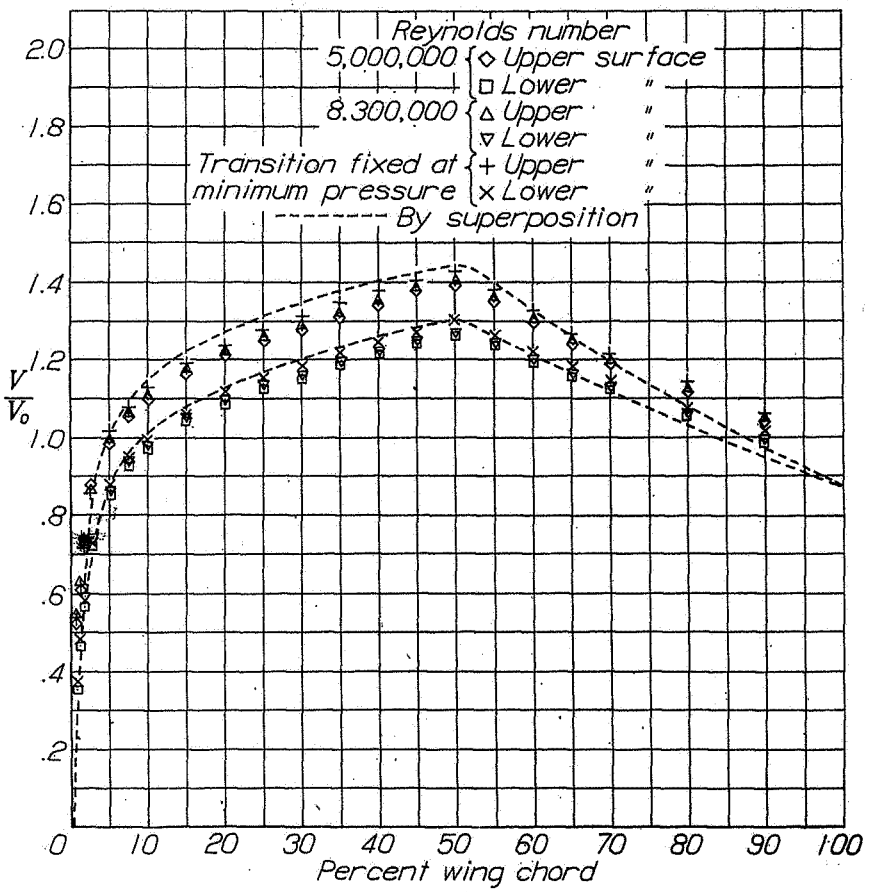

Figure 23.- Velocity distribution in wing-nacelle (NACA 133-30) junction.